Structural studies of the shortest extended synaptotagmin with only two C2 domains from Trypanosoma brucei

Emma Stepinac, Nicolas Landrein, Daria Skwarzyńska, Patrycja Wójcik, Johannes Lesigang, Iva Lučić, Cynthia He, Melanie Bonhivers, Derrick R Robinson, Gang Dong

iScience

CellPress
OPEN ACCESS

Article

Structural studies of the shortest extended synaptotagmin with only two C2 domains from *Trypanosoma brucei*

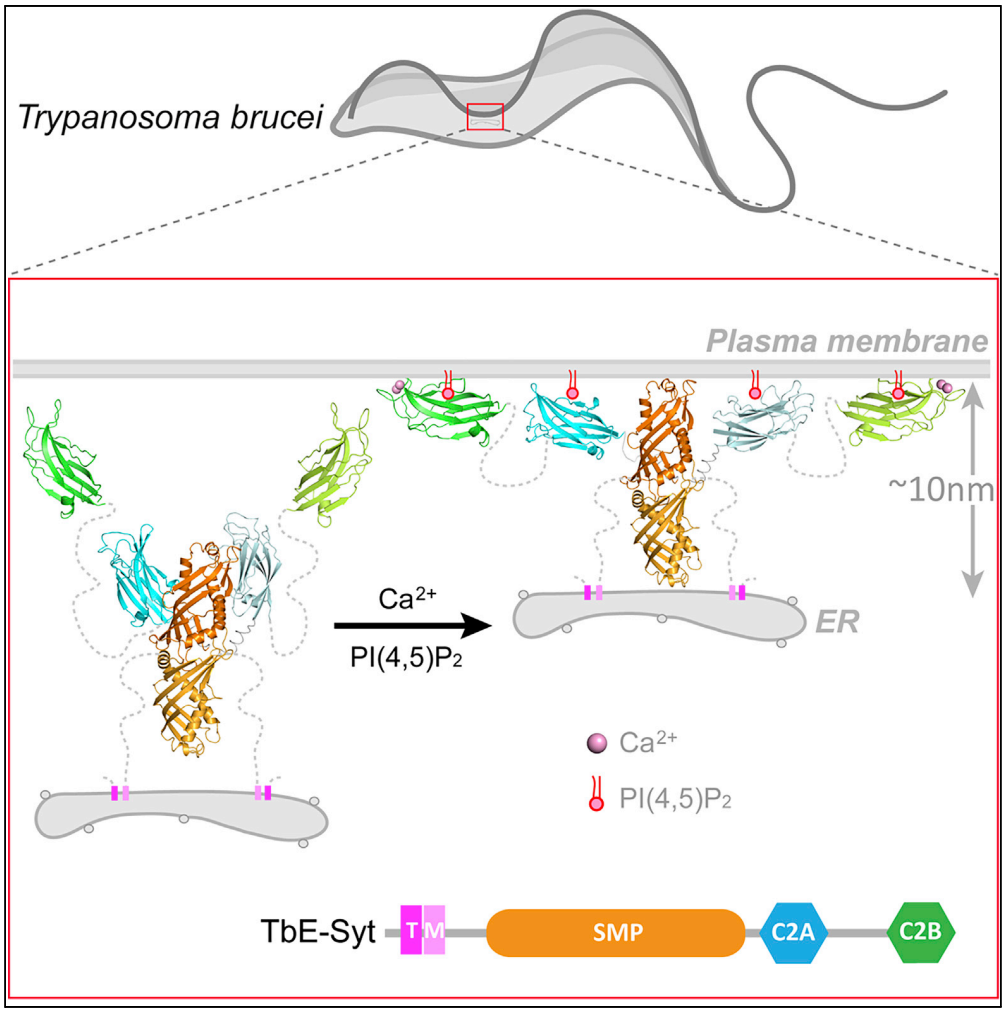

Emma Stepinac, Nicolas Landrein, Daria Skwarzyńska, ..., Mélanie Bonhivers, Derrick R. Robinson, Gang Dong

gang.dong@meduniwien.ac.at

Highlights

We identified a new type of extended synaptotagmin (E-Syt) in *Trypanosoma brucei*

TbE-Syt is the shortest known E-Syt with only two C2 domains, C2A and C2B

TbE-Syt-C2B binds lipids via both Ca^{2+}- and PI(4,5)P_2-dependent means

Unlike all other known E-Syts, TbE-Syt-C2A and C2B are connected by a flexible loop

Stepinac et al., iScience *24*, 102422
May 21, 2021
https://doi.org/10.1016/j.isci.2021.102422

iScience

CellPress
OPEN ACCESS

Article

Structural studies of the shortest extended synaptotagmin with only two C2 domains from *Trypanosoma brucei*

Emma Stepinac,[1] Nicolas Landrein,[2] Daria Skwarzyńska,[1,3] Patrycja Wójcik,[1,3] Johannes Lesigang,[1] Iva Lučić,[1,5] Cynthia Y. He,[4] Mélanie Bonhivers,[2] Derrick R. Robinson,[2] and Gang Dong[1,6,*]

SUMMARY

Extended synaptotagmins (E-Syts) localize at membrane contact sites between the endoplasmic reticulum (ER) and the plasma membrane to mediate inter-membrane lipid transfer and control plasma membrane lipid homeostasis. All known E-Syts contain an N-terminal transmembrane (TM) hairpin, a central synaptotagmin-like mitochondrial lipid-binding protein (SMP) domain, and three or five C2 domains at their C termini. Here we report an uncharacterized E-Syt from the protist parasite *Trypanosoma brucei*, namely, TbE-Syt. TbE-Syt contains only two C2 domains (C2A and C2B), making it the shortest E-Syt known by now. We determined a 1.5-Å-resolution crystal structure of TbE-Syt-C2B and revealed that it binds lipids via both Ca^{2+}- and $PI(4,5)P_2$-dependent means. In contrast, TbE-Syt-C2A lacks the Ca^{2+}-binding site but may still interact with lipids via a basic surface patch. Our studies suggest a mechanism for how TbE-Syt tethers the ER membrane tightly to the plasma membrane to transfer lipids between the two organelles.

INTRODUCTION

Eukaryotic cells are compartmentalized into membrane-bound organelles, which are defined by their unique membrane lipid composition and specific functions. Membrane trafficking acts to transfer materials between organelles over long distances, whereas closely apposed membranes from two organelles can form membrane contact sites (MCSs) to exchange lipids between them without undergoing membrane fusion (Hayashi et al., 2008; Lahiri et al., 2015; Levine and Loewen, 2006). Extended synaptotagmins (E-Syts) are a family of evolutionarily conserved proteins localizing at the MCS between the endoplasmic reticulum (ER) and the plasma membrane and mediate lipid transfer between them (Fernandez-Busnadiego et al., 2015; Giordano et al., 2013). E-Syts belong to the tubular lipid binding (TULIP) superfamily. Proteins from this group contain hydrophobic tunnels in their TULIP domains and often function in lipid traffic and signaling by carrying lipids through the aqueous phase of the cell (Beamer et al., 1997; Kopec et al., 2011; Qiu et al., 2007; Wong and Levine, 2017). The name of E-Syt derives from synaptotagmin (Syt), which is a protein anchored on the membrane of secretory vesicles and acting as a tether between the vesicles and their target sites during exocytosis (Brose et al., 1992; Elferink et al., 1993; Perin et al., 1991). However, E-Stys differ from Syts in both their localization and function.

E-Syts are present in plants, fungi, and animals (Craxton, 2007; Giordano et al., 2013; Toulmay and Prinz, 2012). There are three E-Syts, E-Syt1, 2 and 3, in mammals (Min et al., 2007). These E-Syts all have two tandem hydrophobic helices at their N terminus, which form a transmembrane (TM) hairpin anchoring them within the ER membrane (Giordano et al., 2013). The E-Syts also contain a central SMP (synaptotagmin-like mitochondrial-lipid binding protein) domain and five (E-Syt1) or three (E-Syt2 and 3) C2 domains at their C terminus (Min et al., 2007). The first two C2 domains, C2A and C2B, of human E-Syt2 (HsE-Syt2) form a rigid V-shaped conformation, with only C2A capable of binding Ca^{2+} (Xu et al., 2014). HsE-Syt2 also forms a homodimer via its SMP domain, which generates a hydrophobic tunnel along the dimer for lipid binding and transfer between the ER and the plasma membrane (Schauder et al., 2014).

Trypanosomes are kinetoplastids that are thought to be one of the earliest branching lineages of eukaryotes (Simpson et al., 2006). Consequently, they are among the most divergent eukaryotes on the planet.

[1]Max Perutz Labs, Vienna Biocenter, Center for Medical Biochemistry, Medical University of Vienna, 1030 Vienna, Austria

[2]University of Bordeaux, CNRS, Microbiologie Fondamentale et Pathogénicité, UMR 5234, 33000 Bordeaux, France

[3]Silesian University of Technology, Gliwice, Poland

[4]Department of Biological Sciences, Center for BioImaging Sciences, National University of Singapore, Singapore, Singapore

[5]Present address: Leibniz Forschungsinstitut für Molekulare Pharmakologie, Berlin, Germany

[6]Lead contact

*Correspondence: gang.dong@meduniwien.ac.at

https://doi.org/10.1016/j.isci.2021.102422

Studies on conserved proteins in trypanosomes could thus help us understand the fundamental function and evolution of these proteins. Here we report our structural and functional characterization of a unique, single-copy E-Syt from *Trypanosoma brucei*.

Similar to all mammalian E-Syts, *T. brucei* E-Syt (TbE-Syt, Tb927.10.13740) is predicted to also have an N-terminal TM hairpin and a central SMP domain, which is a defining element of the E-Syt protein family. However, TbE-Syt contains only two C2 domains, which we named C2A and C2B based on their topological and structural similarities to their counterparts in mammalian E-Syts. We determined a 1.5-Å-resolution crystal structure of TbE-Syt-C2B, which revealed that it adopts a type II topology and has two tightly bound Ca^{2+} ions. These Ca^{2+} ions are coordinated by a few negatively charged residues from two extended loops. Additionally, the structure shows an extensive surface patch consisting of mostly basic residues. Our *in vitro* liposome-binding data demonstrated that TbE-Syt-C2B bound lipids via both Ca^{2+}-dependent and phosphatidylinositol 4,5-bisphosphate [$PI(4,5)P_2$]-dependent means through these two sites. Homology modeling analyses showed that TbE-Syt-C2A lacks Ca^{2+}-binding sites, which is distinct from the Ca^{2+}-binding C2A in all mammalian E-Syts. However, TbE-Syt-C2A also contains a similar basic patch to that on TbE-Syt-C2B. Furthermore, our analyses suggest that TbE-Syt-C2A and C2B are connected by a flexible linker, which is also different from the rigid and compact V-shaped conformation of C2A-C2B in mammalian E-Syts. TbE-Syt localized to a specialized ER subdomain in *T. brucei*, and these distinct features of TbE-Syt may correlate with its functions there.

RESULTS

TbE-Syt localizes to the ER via its N-terminal transmembrane hairpin

The gene Tb927.10.13740 from *T. brucei* encodes a protein of 594 residues and was previously annotated as a putative synaptotagmin (Aslett et al., 2010). Our preliminary bioinformatics analyses suggested that this protein contains two TM motifs (aa14–31 and 34–56), an SMP domain (aa100-280), and two C2 domains (C2A: aa290–420; C2B: aa474–594) (Figure 1A). Sequence alignment of homologs from various trypanosome species showed that all these domains, except for the first TM motif, are highly conserved, whereas the short N-terminal extension and the connecting loop between the two C2 domains are both divergent and variable in length (Figure 1B). Based on its similar overall domain organization to mammalian E-Syts and characteristic localization to the cortical ER revealed by our studies, we provisionally renamed this protein *T. brucei* E-Syt (TbE-Syt).

To assess the localization of TbE-Syt in *T. brucei*, we generated a cell line which inducibly overexpressed TbE-Syt-myc and domains and analyzed by western blotting (WB) the whole cell (WC) or the cytoskeleton-associated fraction of detergent-extracted cells (CSK). The expression level was different among the constructs preventing further WB quantitative comparison (Figures S1A and S1B). However, the analysis showed that both TbE-Syt (FL) and TbE-Syt deleted of the C2B domain (T1) co-purified with the CSK fraction, whereas both the C2B domain (T2) and the TM domain (T3) alone were only found in WC suggesting no or poor CSK association. Nevertheless, the TM domain is required for CSK association as TbE-Syt deleted of its TM (T4) or deleted of both TM and C2B domains (T5) were all soluble.

BiP, which is a molecular chaperone located in the ER lumen, was chosen as an ER marker (Bangs et al., 1993) (Figure 2A, panel a). Co-immunolabeling of BiP and TbE-Syt-myc demonstrated that TbE-Syt co-localizes with BiP at the ER with a Pearson's coefficient (PC) of 0.93 $\pm$ 0.04 (Figures 2A, panel b, and S1C). Similarly, TbE-Syt-YFP also localized to the ER in the cell (Figure S2). The C2B domain was not involved in TbE-Syt localization as its deletion or mutation did not change the ER localization of the protein (the PCs were 0.89 $\pm$ 0.06 and 0.89 $\pm$ 0.10 for T1 and mutC2B, respectively) (Figures 2A, panel c, and S1C, T1 and mutC2B). As expected, when C2B was expressed alone, it was cytosolic (Figures 2A, panel d, and S1C, T2). Notably, although the TM alone co-localized with BiP at the ER (PC 0.96 $\pm$ 0.02), it disappeared in the extracted cytoskeletons (Figures 2A, panel e, and S1C, T3). Conversely, the construct lacking the TM was completely cytosolic (Figures 2A, panel f).

Besides the central ER that is connected to the nuclear envelope, the same as in canonical eukaryotes, trypanosomes have an extra unique flagellar attachment zone (FAZ)-associated cortical ER (Sherwin and Gull, 1989; Vickerman, 1969). In detergent-extracted cells (i.e., cytoskeletons), labeling of full-length TbE-Syt-myc remained along the flagellum up to the anterior end of the cell body (Figure S1C) and was detected in the cytoskeleton fraction by WB (Figure S1B). We therefore further checked whether TbE-Syt localizes

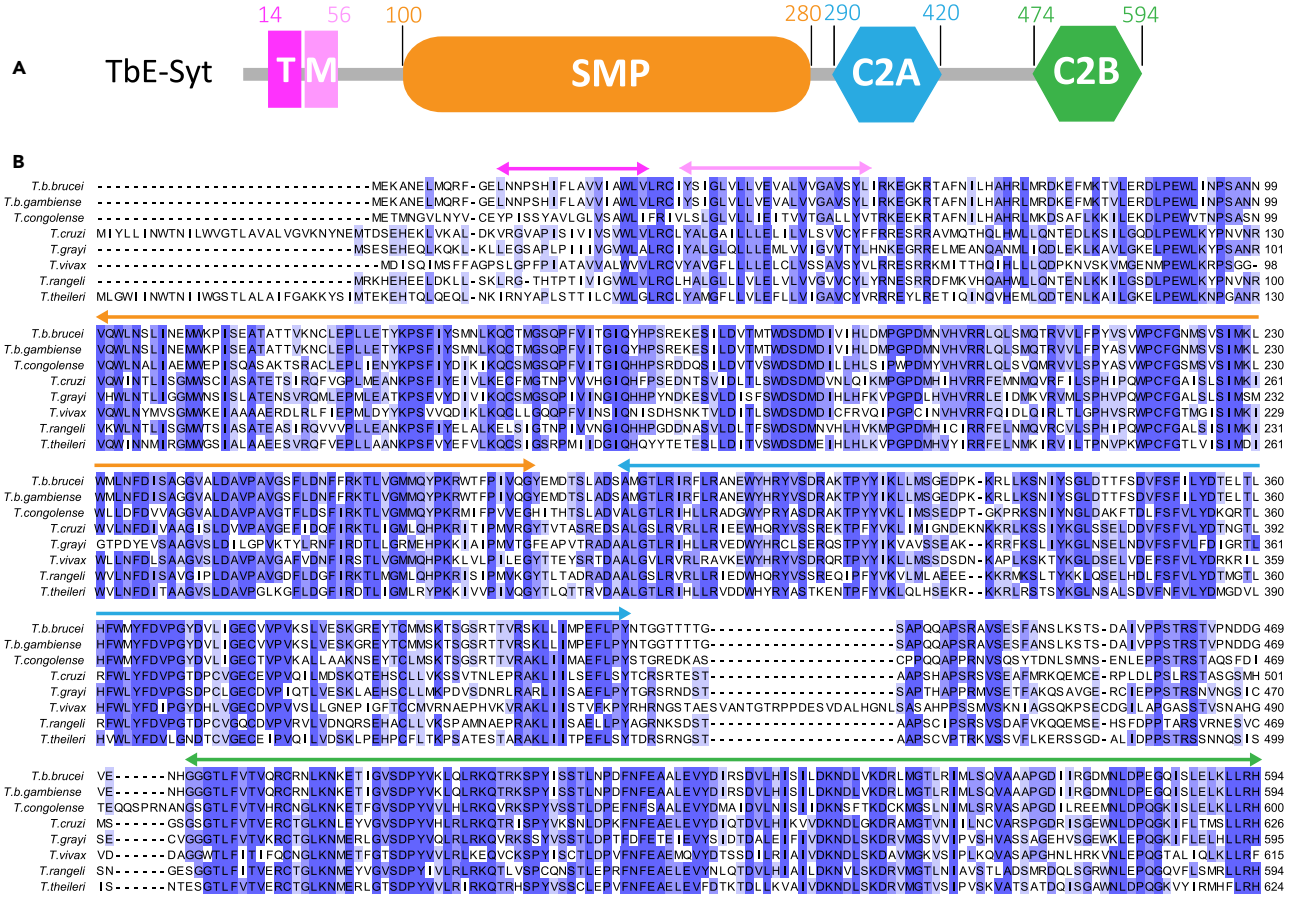

Figure 1. Domain arrangement and conservation analyses of TbE-Syt

(A) Schematic illustration of the predicted domains in TbE-Syt. Amino acids in primary structure are shown above the schematic.

(B) Sequence alignments of TbE-Syt homologs from various trypanosome species. Boundaries of the predicted domains are marked by arrows above the sequences with the same color schemes as in (A). The alignments were carried out using the option of "Muscle with defaults" in Jalview, with shading indicating the degree of conservation.

to the FAZ-associated ER using another *T. brucei* cell line stably expressing C-terminally YFP-tagged TbE-Syt. Two antibodies, anti-PFR2 (L8C4) and anti-FAZ1 (L3B2), were chosen to mark the whole flagellum and the FAZ, respectively (Gadelha et al., 2005; Kohl et al., 1999). Our immunofluorescence data showed that TbE-Syt overlapped with PFR2 along the flagellum, but the signal did not reach the flagellar tip (Figure 2B). TbE-Syt overlapped with FAZ1 along the entire FAZ, however (Figure 2C). This is consistent with the FAZ localization of TbE-Syt reported in a high-throughput screening database where the majority of C-terminally mNeonGreen-tagged TbE-Syt was observed in the FAZ area, with some weak signals forming reticulated patches in the cytoplasm (Dean et al., 2017) (Figure S3).

To further verify its association with the ER, we checked TbE-Syt localization at the ultrastructural level by immuno-gold labeling. The results showed that TbE-Syt localized to both the FAZ-associated ER beneath the flagellum and the central ER around the nuclear envelope (Figure 2D). Overall, our data confirm that TbE-Syt localizes primarily to the FAZ-associated ER in *T. brucei*, and correct localization is mainly mediated by its N-terminal TM domains.

Homology modeling suggests that TbE-Syt-SMP is capable of binding lipids

The SMP domain is the signature element of all E-Syts. However, none of the TbE-Syt constructs containing the SMP domain we generated produced soluble recombinant protein, which prevented us from carrying out *in vitro* biochemical and structural studies on this critical domain. To understand the structure and function of TbE-Syt-SMP, we turned to bioinformatics analyses to generate a homology model for it. The top hit

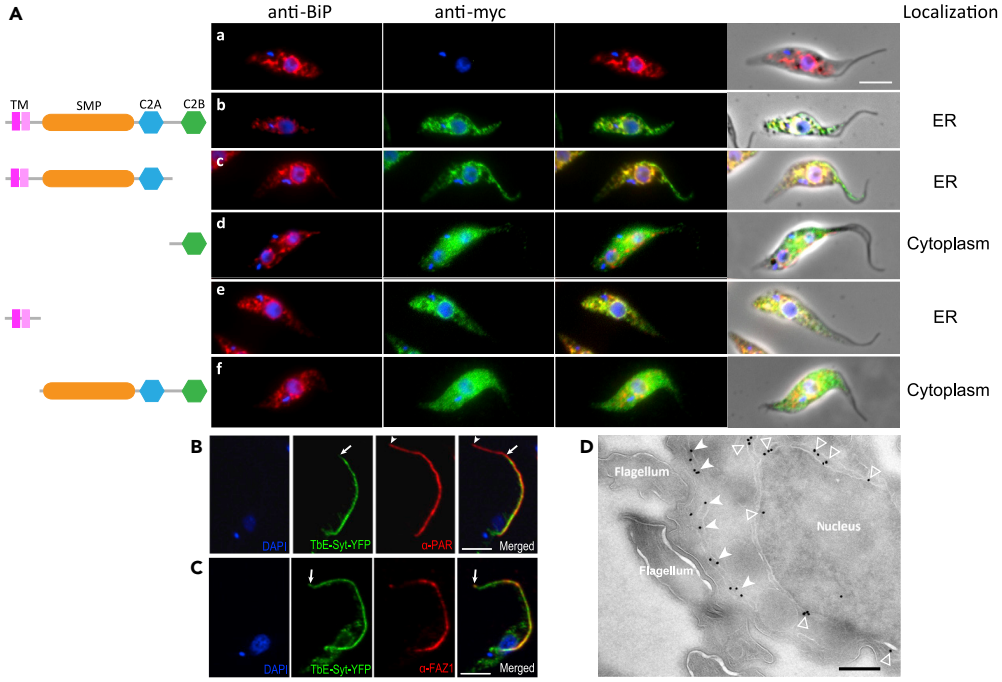

Figure 2. TbE-Syt localizes to the ER

(A) TbE-Syt colocalizes with BiP at the ER via its N-terminal transmembrane domain. *T. brucei* procyclic form cells (parental, a) and those expressing various truncations of myc-tagged TbE-Syt (b–f) were probed by immunofluorescence with BiP (red) and anti-myc (green) antibodies. Kinetoplasts and nuclei were stained with DAPI. Scale bar, 5 μm.

(B and C) Cells stably expressing TbE-Syt-YFP were stained with DAPI for DNA and labeled with anti-PAR (α-PAR) antibodies for the entire flagellum (B) or with anti-FAZ1 (α-FAZ1) for the FAZ (C). Images were acquired with an LSM510 Meta confocal microscope. The tips of the FAZ and the flagellum are marked by arrows and arrowheads, respectively. Scale bars, 5 μm.

(D) Immunogold labeling of TbE-Syt-YFP cells using anti-GFP antibodies. Gold particles were associated both with the central ER around the nuclear envelope (open arrowheads) and with the FAZ-associated ER beneath the flagellum (arrowheads). Scale bar, 200 nm.

See also Figures S1–S3.

identified by the protein structure homology-modeling program SWISS-MODEL Workspace (Waterhouse et al., 2018) was the crystal structure of the SMP domain of HsE-Syt2, which was solved to 2.4 Å resolution with bound phospholipids (PDB: 4P42) (Schauder et al., 2014). We chose this crystal structure, which shares 20.45% identity with TbE-Syt-SMP, as the template for our homology modeling (Figures 3A and S4A).

The resulting homodimeric model was of high quality based on the confidence evaluation and local similarity to the template (Figures S4B and S4C). Superimposing the TbE-Syt-SMP model onto the template structure of HsE-Syt2-SMP showed an excellent agreement (Figure 3B). The homodimeric TbE-Syt-SMP model, which was generated using the quaternary structure prediction option of SWISS-MODEL (Bertoni et al., 2017) with lipids extracted from the superimposed template structure, predicted that the lipid molecules would bind in a deep cleft between the long α helix and the edge of the extended β sheet (Figure 3C). This cleft consists almost exclusively of hydrophobic residues that are highly conserved in all trypanosomes, which suggests that TbE-Syt-SMP has the capability of binding lipids in a similar fashion to the SMP domain of HsE-Syt2 (Figures 3D and 3E).

The TbE-Syt C2B domain contains a conserved Ca^{2+}-binding site

In contrast to mammalian E-Syts that have at least three C2 domains, TbE-Syt contains only two C2 domains. To further characterize the structure and function of TbE-Syt, we first determined a crystal structure for its C2B domain (Figure 4A). The structure was solved to 1.5 Å resolution using the selenium single-wavelength anomalous diffraction *de novo* phasing method (Table 1). There are two molecules *per* asymmetric

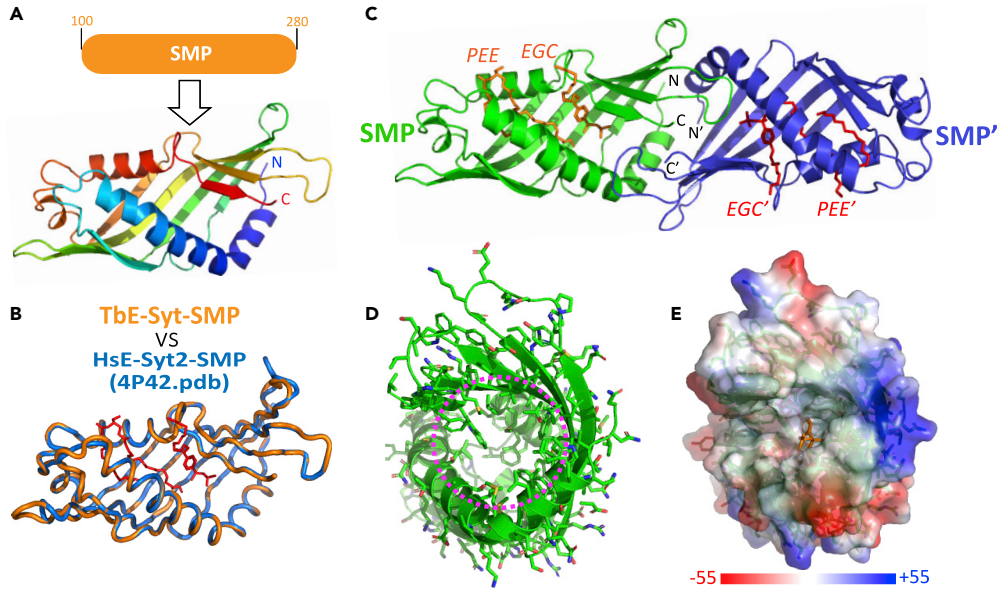

Figure 3. Homology modeling of the SMP domain of TbE-Syt

(A) Modeling of the SMP domain (aa100–280) by SWISS-MODEL using the crystal structure of HsE-Syt2 (PDB: 4P42) as the template.

(B) TbE-Syt-SMP model (orange) superimposed onto the modeling template (marine). The lipid molecules in the HsE-Syt2 structure are shown as red sticks.

(C) Inferred dimeric assembly of TbE-Syt-SMP based on the crystal structure of HsE-Syt2.

(D) End view of TbE-Syt-SMP in (A) seen from the right side. The interior of the structure (purple circle) contains mostly hydrophobic residues.

(E) Electrostatic surface of TbE-Syt-SMP in the same orientation as in (D). Lipid molecules extracted from the superimposed HsE-Syt2 structure are shown as orange sticks. All images were prepared using PyMOL.

See also Figure S4.

unit, both of which contain aa474-594 of TbE-Syt. The two molecules are essentially identical, with an average root-mean-square deviation (RMSD) of 0.25 Å for all aligned backbone atoms.

The structure showed that TbE-Syt-C2B adopts a type II topology, consisting of eight β strands that form two sheets and a short α helix in the loop connecting β6 and β7 (Figure 4B). Additionally, there are two tightly bound Ca^{2+} ions, which are coordinated by a few charged residues in two extended loops on the opposite end from the helix (Figure 4C). The interaction is mediated by a network of hydrogen bonds between the Ca^{2+} ions and the side-chain oxygens of residues E492, D498, D545, and N547, which are all highly conserved in trypanosomes (Figure 4D). The main-chain carboxyl oxygens of residues V496 and K546 also form hydrogen bonds with either of the two Ca^{2+} ions. Additionally, there are four stably bound water molecules hydrogen bonded to these two Ca^{2+} ions (Figure S5).

TbE-Syt-C2B binds lipids in both Ca^{2+}- and $PI(4,5)P_2$-dependent manners

Similar to the Ca^{2+}-binding site in the C2A domain of HsE-Syt2, TbE-Syt-C2B also has an extremely acidic "crater" on its surface (Figure 5A). Previous studies showed that the C-terminal C2 domain of mammalian E-Syt2 and E-Syt3 interacts with the plasma membrane via a basic surface patch (Giordano et al., 2013). In the TbE-Syt-C2B structure there is also a basic patch on β2 and β3, which contains residues K502 and K511 at its center (Figure 5B). Additionally, there is a highly conserved aromatic residue, Y500, at the deepest point of this curved patch. Both the basic patch and the conserved Y500 residues are reminiscent of the C2 domain of PKCα that associates with $PI(4,5)P_2$ via a similar basic patch (Guerrero-Valero et al., 2009).

To check whether TbE-Syt-C2B interacts with lipids through either or both the Ca^{2+}-binding site and the basic patch, we generated two types of mutations. In one mutant, we abolished Ca^{2+} binding by mutating residues E492 and D498, which are simultaneously hydrogen bonded with both Ca^{2+} ions, to alanine

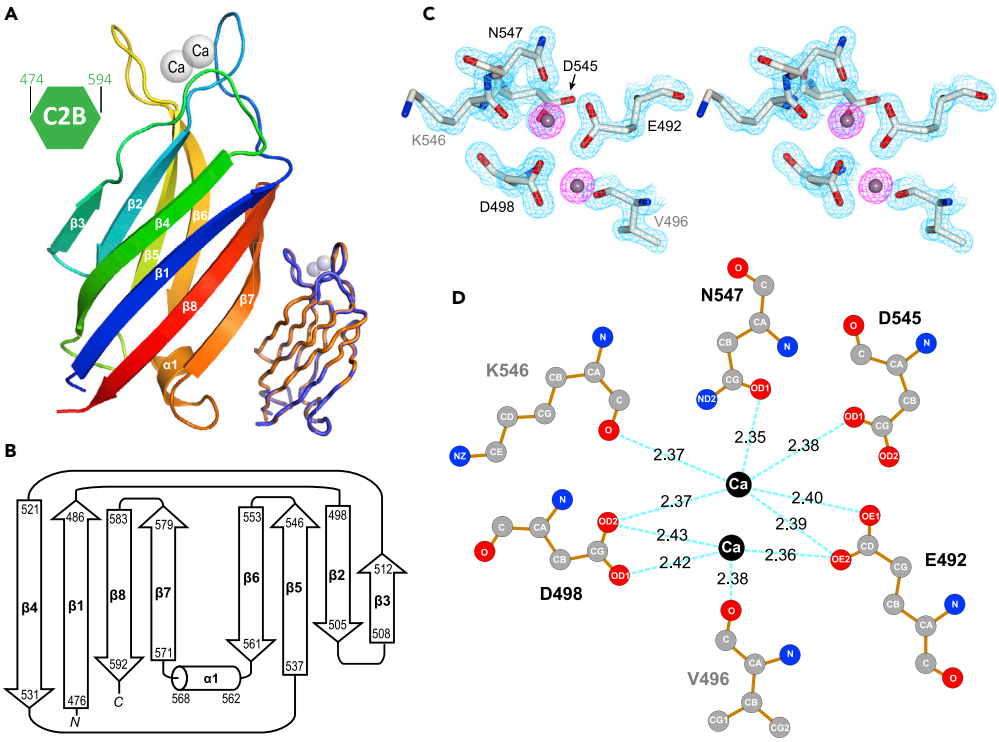

Figure 4. Crystal structure of the C2B domain of TbE-Syt

(A) Ribbon diagram of the TbE-Syt-C2B crystal structure color-ramped from blue at the N terminus to red at the C terminus. Secondary structures and the two bound Ca^{2+} ions (gray spheres) are labeled. The two molecules in the asymmetric unit are shown superimposed in the lower right corner.

(B) Secondary structure diagram of TbE-Syt-C2B, with the residue ranges of each structural element indicated.

(C) Stereo view of the *2Fo-Fc* map around the Ca^{2+}-binding site contoured at 2 σ level. Electron densities around the Ca^{2+} ions are highlighted in purple. The plot was produced using CCP4mg (McNicholas et al., 2011).

(D) Hydrogen bonds between the Ca^{2+} ions and coordinating residues in TbE-Syt-C2B. The plot was generated using LigPlot+ (Laskowski and Swindells, 2011).

See also Figure S5.

(E492A/D498A). In another mutant, we changed the two lysine residues at the center of the basic patch to opposite charges, i.e., K502E/K511E. Additionally, we generated a combined mutant for all these residues, E492A/D498A/K502E/K511E.

We used *in vitro* liposome binding assays to investigate whether TbE-Syt-C2B binds liposomes and, if so, whether any of the mutants affect this interaction. Purified wild-type and mutant proteins were incubated with sucrose-loaded vesicles containing different molar ratios of lipids and pelleted at high speed to separate the liposome-bound and unbound fractions of the proteins. SDS-PAGE analyses of the supernatant (unbound) and pellet (liposome-bound) fractions showed that wild-type TbE-Syt-C2B bound liposomes very weakly in the absence of both Ca^{2+} and $PI(4,5)P_2$ (Figure 5C, WT: lane 4). However, addition of either Ca^{2+} or $PI(4,5)P_2$ to the reaction showed robust binding (Figure 5C, WT: lanes 6 and 8). Notably, protein bound to liposomes was slightly more abundant when both Ca^{2+} and $PI(4,5)P_2$ were present (Figure 5C, WT: lane 10). The mutant E492A/D498A abolished only the Ca^{2+}-dependent lipid binding, but not $PI(4,5)P_2$-mediated binding (Figure 5C, lane 6 versus lane 8). Interestingly, addition of Ca^{2+} abolished the $PI(4,5)P_2$-mediated liposome binding of this mutant even though $PI(4,5)P_2$ was present on the liposomes (lane 10). This was probably because excessive Ca^{2+} ions would bind to the negatively charged head groups of $PI(4,5)P_2$ and thus shielded the interaction of the basic patch with the lipid. The converse effect was observed for the basic patch mutant (K502E/K511E), which retained the Ca^{2+}-dependent liposome binding while completely losing $PI(4,5)P_2$-lipid binding ability (Figure 5C, lane 6 versus lane 8). This indicated that TbE-Syt-C2B binds liposomes in two different fashions. Indeed, only upon mutating both Ca^{2+}-binding and the central basic patch residues (E492A/D498A/K502E/K511E) was the liposome binding of TbE-Syt-C2B completely abolished.

Table 1. Data collection and refinement statistics

Data collection	
Space group	$P2_12_12_1$
Wavelength (Å)	0.873
Cell dimensions	
a, *b*, *c* (Å)	54.91, 57.53, 84.57
Resolution (Å)	50.0–1.50 (1.55–1.50)[a]
Total reflections	232,968 (23,835)
Unique reflections	43,464 (4,297)
Multiplicity	5.4 (5.5)
R_{merge}	0.083 (0.978)
R_{meas}	0.092 (1.035)
R_{pim}	0.039 (0.429)
CC(1/2)	0.998 (0.644)
CC[a]	0.999 (0.885)
Mean $I/\sigma(I)$	10.39 (1.37)
Completeness (%)	99.6 (99.8)
Wilson B-factor	17.08
Refinement	
Resolution (Å)	20–1.50
Number of reflections	43,445
R_{work}/R_{free} (%)	16.97/19.13
No. atoms	
Protein	1,986
Water	353
Ligand/ion	16
B-factors	
Protein	22.7
Water	36.7
Ligand/ion	24.7
RMSD	
Bond lengths (Å)	0.012
Bond angles (°)	1.221
Ramachandran plot	
Favored (%)	100.00
Allowed (%)	0
Outlier (%)	0

[a]Values in parentheses are for the highest resolution shell.

TbE-Syt-C2A lacks the Ca^{2+}-binding site but retains the $PI(4,5)P_2$-binding patch

Previous studies have shown that the C2A domain in all mammalian E-Syts binds Ca^{2+} and is involved in lipid interaction (Min et al., 2007; Xu et al., 2014). We wondered whether TbE-Syt-C2A functions similarly. We tried to express recombinant TbE-Syt-C2A, either alone or together with C2B, SMP, or both, but did not succeed in obtaining soluble proteins. We thus tried to understand its structure and function by homology modeling. One of the top hits recognized by SWISS-MODEL (Waterhouse et al., 2018) was the crystal structure of HsE-Syt2-C2A (PDB: 4NPK) (Xu et al., 2014), which shares ~17% identity with TbE-Syt-C2A. High local similarity of the final model and consistent alignment of secondary structures between the model and the template suggested that it is a convincing homology model (Figures 6A and S6). Superimposing the TbE-Syt-C2A model onto the HsE-Syt2-C2A crystal structure also showed an overall very good agreement (Figure 6B).

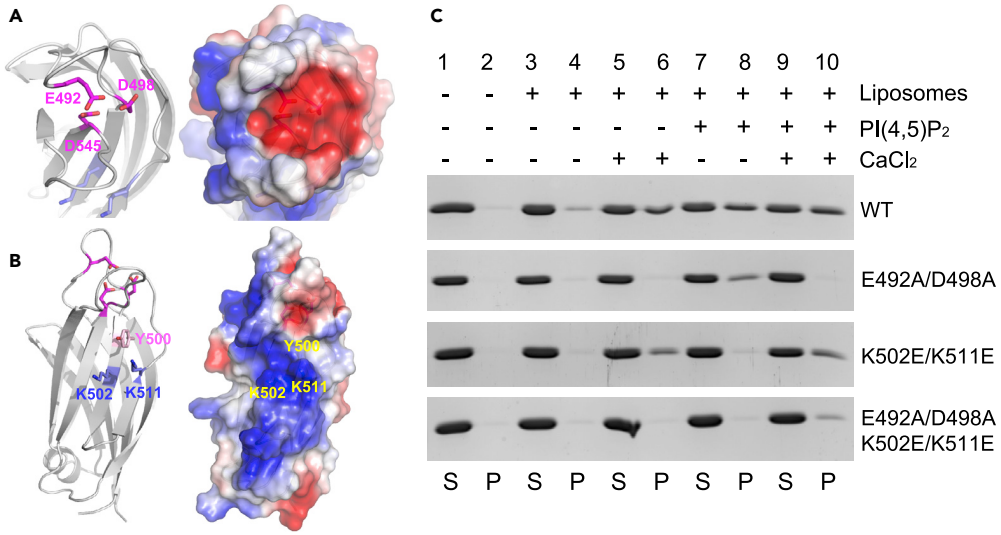

Figure 5. TbE-Syt-C2B binds lipids using two distinct sites

(A) Ribbon (left) and electrostatic (right) plots of the Ca^{2+}-binding acidic patch in the TbE-Syt C2B domain. The three highly conserved acidic residues in the core of the patch are shown as sticks and labeled. Ca^{2+} ions are omitted for clarity.

(B) Side view of TbE-Syt-C2B with the two basic residues in the center of the positively charged patch labeled.

(C) Liposome pelleting assays of wild-type (WT) and three mutants of TbE-Syt-C2B in the presence or absence of $PI(4,5)P_2$ and/or $CaCl_2$. S: supernatant; P: pellet.

The previously reported crystal structure of HsE-Syt2-C2A contains three tightly bound Ca^{2+} ions coordinated by six Asp residues from two connecting loops via an extensive hydrogen bond network. This site is responsible for the binding of HsE-Syt2-C2A to lipids (Xu et al., 2014). Surprisingly, close examination of the putative Ca^{2+}-binding site of TbE-Syt-C2A in the superimposed structures revealed that five of the six Asp residues in HsE-Syt2-C2A are substituted by hydrophobic residues in TbE-Syt-C2A (Figure 6C). Consequently, the concave acidic patch for Ca^{2+} binding present in HsE-Syt2-C2A (Figure 6D) was replaced by a saddle-like hydrophobic area in TbE-Syt-C2A (Figure 6E). This suggests that the C2A domain in TbE-Syt is unlikely to bind Ca^{2+}.

Previous studies showed that C2A and C2B of HsE-Syt2 share a similar conformation (Xu et al., 2014). We superimposed the homology model of TbE-Syt-C2A onto the crystal structure of TbE-Syt-C2B and found that not only was their overall conformation very similar but also the $PI(4,5)P_2$-binding site was present in both C2 domains (Figures 6F and 6G). As shown above, we have found that TbE-Syt-C2B interacts with lipids in both Ca^{2+}- and $PI(4,5)P_2$-mediated fashions (Figure 5C). The highly conserved basic patch on TbE-Syt-C2A suggests that, despite lacking a Ca^{2+}-binding site, it might be still involved in lipid binding via the $PI(4,5)P_2$-dependent mode (Figure 6H).

TbE-Syt-C2A and C2B are connected by a long flexible loop

Previous structural studies revealed that the first two C2 domains, i.e., C2A and C2B, of HsE-Syt2 shares high structural similarities with each other (Xu et al., 2014). A high-resolution NMR structure of the last C2 domain of HsE-Syt2, i.e., C2C, has also been determined (PDB: 2DMG). We therefore compared the structure of TbE-Syt-C2B with that of the three C2 domains of HsE-Syt2. TbE-Syt-C2B adopts the same topology as HsE-Syt2-C2A and C2B, i.e., type II, whereas HsE-Syt2-C2C has a distinct type I topology (Figure S7A). Superimposing TbE-Syt-C2B onto each of the three C2 domains of HsE-Syt2 showed that it is very similar to HsE-Syt2-C2A and C2B, with average RMSDs of 1.05 Å and 0.75 Å, respectively, but substantially deviated from C2C, with an RMSD of 3.57 Å (Figures S7B and S7C). This further confirms that the C2A and C2B domains in TbE-Syt are equivalent to C2A and C2B of HsE-Syt2.

HsE-Syt2-C2A and C2B fold into a compact V-shaped conformation, which is stabilized by the antiparallel interaction of the C termini of the last β strands on these domains (Xu et al., 2014) (Figure 7A). Structural comparison with HsE-Syt2-C2A-C2B showed that the last β strands of both TbE-Syt-C2A and C2B are

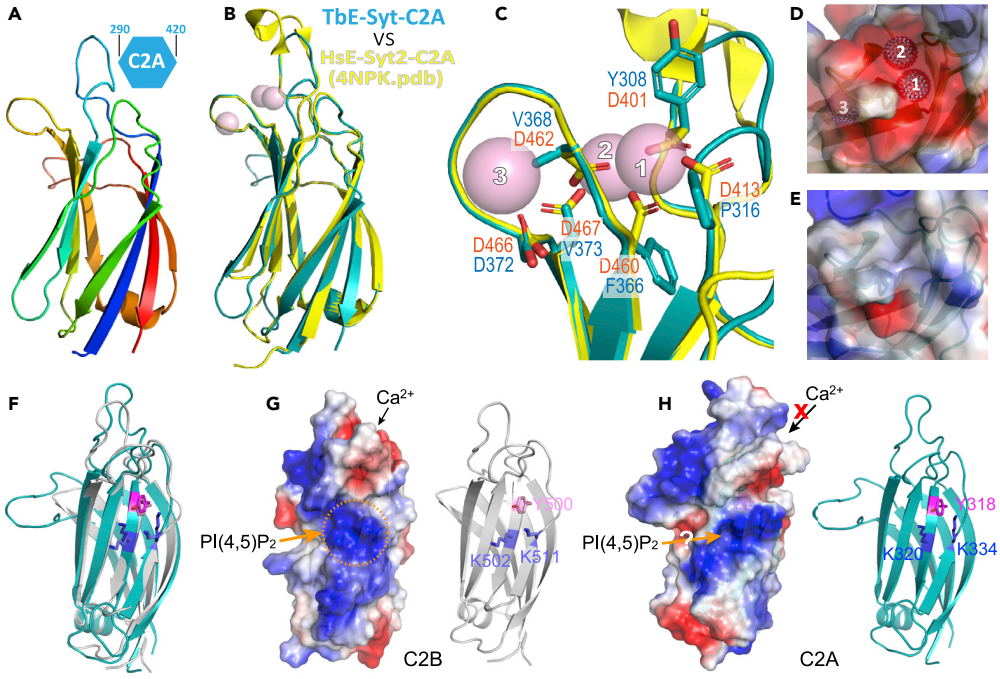

Figure 6. Homology modeling of the TbE-Syt C2A domain

(A) Modeling of TbE-Syt-C2A (aa290–420) by SWISS-MODEL using the homologous structure of the HsE-Syt2-C2A (PDB: 4NPK) as the template.

(B) TbE-Syt-C2A model (cyan) superimposed onto the modeling template (yellow). The three Ca^{2+} ions in the template structure are shown as pink spheres.

(C) Close-up view of the Ca^{2+}-binding site of the superimposed structures in (B). Residues in HsE-Syt2 coordinating Ca^{2+} ions (pink spheres) are shown as orange sticks, and corresponding residues in TbE-Syt are shown as teal sticks.

(D) Electrostatic plot of the Ca^{2+}-binding site of HsE-Syt2, with the three Ca^{2+} ions shown as labeled spheres.

(E) Corresponding region in TbE-Syt-C2A in the same orientation as in (D) and with the same electrostatic scale. The putative Ca^{2+}-binding site is mostly hydrophobic in TbE-Syt-C2A.

(F) Superimposed ribbon diagrams of the C2A model and the C2B crystal structure of TbE-Syt. The three critical residues in the patches for $PI(4,5)P_2$-mediated lipid binding are shown as sticks.

(G) Electrostatic plot and ribbon diagram of TbE-Syt-C2B. Ca^{2+} ions bind to the acidic patch at the top end, and the $PI(4,5)P_2$-binding site is encircled in orange.

(H) Dual plots of TbE-Syt-C2A in the same orientation as (F). The putative Ca^{2+}-binding site is hydrophobic and not able to bind Ca^{2+}, the $PI(4,5)P_2$-binding site is highly conserved. This suggests that TbE-Syt-C2A could potentially binds lipids in the $PI(4,5)P_2$-mediated manner.

See also Figure S6.

too short to allow similar inter-strand interaction between them (Figures 7B and 7C). Therefore, the linker between TbE-Syt-C2A and C2B, which consists of 55 residues (aa419–473), likely forms a long flexible loop. The predicted flexibility of the loop is supported by the folding analysis on TbE-Syt (Figure S8). Local dynamic state of each residue in TbE-Syt was quantitatively evaluated using ODiNPred, which uses a deep neural network trained on experimental NMR-derived *Z* scores and has been shown superior in predicting disordered loops (Dass et al., 2020). ODiNPred strongly suggests that the region spanning aa418–474 in TbE-Syt is exclusively disordered (Figure S8A).

DISCUSSION

We report here our structural characterizations of an uncharacterized E-Syt from *T. brucei*. Our bioinformatics analyses showed that, similar to all known mammalian E-Syts, TbE-Syt also has two TM motifs at its N terminus and a central SMP domain (Figure 1). However, it contains only two C2 domains, in contrast to at least three C2 domains in all other reported E-Syts in animals, plants, and yeast (Craxton, 2007; Giordano et al., 2013; Min et al., 2007; Toulmay and Prinz, 2012). This makes TbE-Syt the shortest E-Syt identified to date.

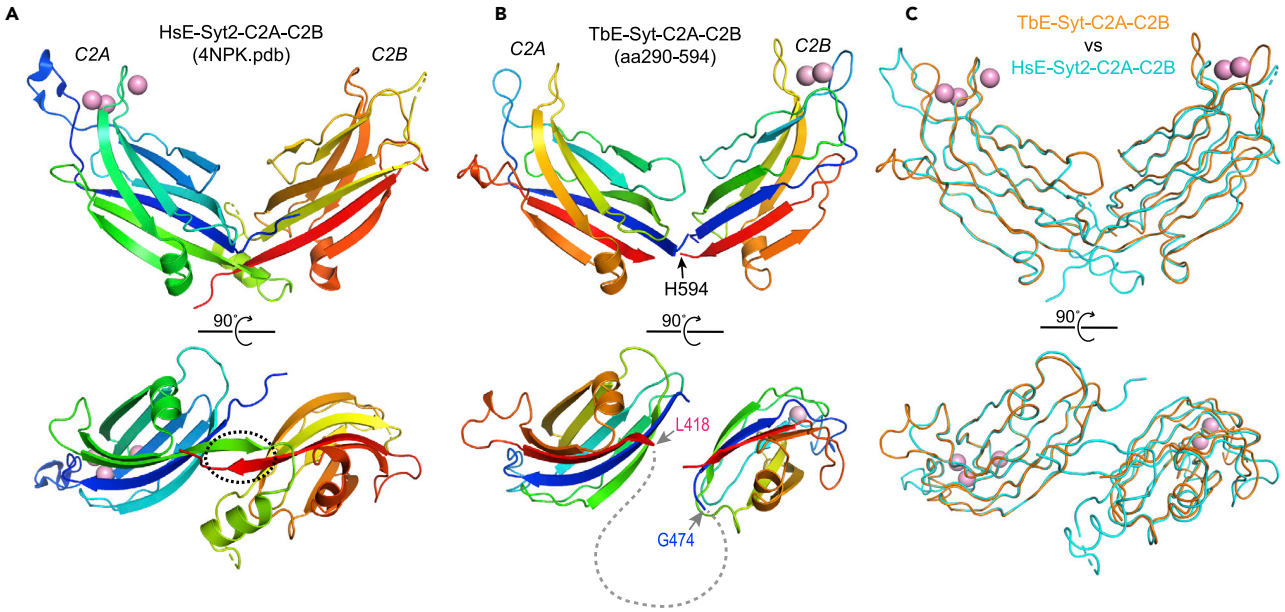

Figure 7. The C2A and C2B domains of TbE-Syt are connected by a long flexible loop

(A) Ribbon diagram of HsE-Syt2-C2A-C2B (PDB: 4NPK), shown in two orientations. The anti-parallel interaction of the last β strand from both domains is indicated with a dashed oval in the lower orientation.

(B) Ribbon diagrams of TbE-Syt-C2A-C2B in the same orientations as in (A). TbE-Syt-C2A is the homology model, and C2B is the crystal structure. H594 is the last residue at the C terminus of TbE-Syt. The last β strands in both TbE-Syt-C2A and C2B are much shorter than those in HsE-Syt2-C2A and C2B and thus not able to make an inter-strand interaction as in HsE-Syt2-C2A-C2B. The long flexible linker is shown as a dashed line.

(C) TbE-Syt-C2A-C2B and HsE-Syt2-C2A-C2B as shown in (A) and (B), superimposed.

See also Figures S7 and S8.

Despite testing several RNAi constructs, RNAi against TbE-Syt in both procyclic and bloodstream forms of *T. brucei* did not decrease the expression of the protein (data not shown), which prevented us from further analyzing its cellular function. Previous systematic high-throughput RNAi screening data showed that depletion of TbE-Syt had no significant effect in bloodstream form *T. brucei*, but deleteriously affected procyclic forms (Figure S9) (Alsford et al., 2011). This suggests that TbE-Syt might play a vital role under certain conditions. Indeed, whereas no severe defects were observed upon their deletion in many organisms (Manford et al., 2012; Saheki et al., 2016; Sclip et al., 2016; Toulmay and Prinz, 2012; Tremblay and Moss, 2016), some specific defects have been observed in yeast, plants, and animals (Aguilar et al., 2007; Levy et al., 2015; Saheki et al., 2016). It is noteworthy that orthologs of TbE-Syt show high synteny in all pathogenic trypanosomes, further suggesting that it is an important gene that has been conserved over evolutionary time.

It was shown previously that in other organisms, including yeast and mammals, E-Syts are selectively concentrated in the cortical ER adjacent to the plasma membrane. This localization can be either constitutive or under the control of the cytosolic Ca^{2+} level (Chang et al., 2013; Giordano et al., 2013; Idevall-Hagren et al., 2015; Manford et al., 2012; Toulmay and Prinz, 2012). Our *in vivo* localization data showed that TbE-Syt localizes to both the central ER close to the nuclear envelope and the FAZ-associated cortical ER beneath the flagellum (Figure 2D). Localization to the central ER was mediated exclusively by the TM motifs as the TM region itself was sufficient to target to the central ER (Figures 2A and S1). However, the TM motifs alone did not localize to the FAZ area and, unlike other longer constructs including full-length and TM-SMP-containing TbE-Syt, were removed in the extracted cells (Figure S1C, T3 construct). It is noteworthy that most tagged TbE-Syts used in our studies were overexpression constructs, which often yield a much higher expression level than that of the endogenous proteins. Notably, the expression levels were also different among constructs, preventing quantitative comparison in WB and immunofluorescence experiments. Tube-like connections have been observed between the FAZ-associated ER and the central ER around the outer nuclear membrane (Lacomble et al., 2009). At an elevated expression level, a fraction of TbE-Syt might also redistribute to the central ER through such tube-like connections. Notably, TbE-Syt has been independently found to localize to the FAZ area and associate with CIF1, a protein present

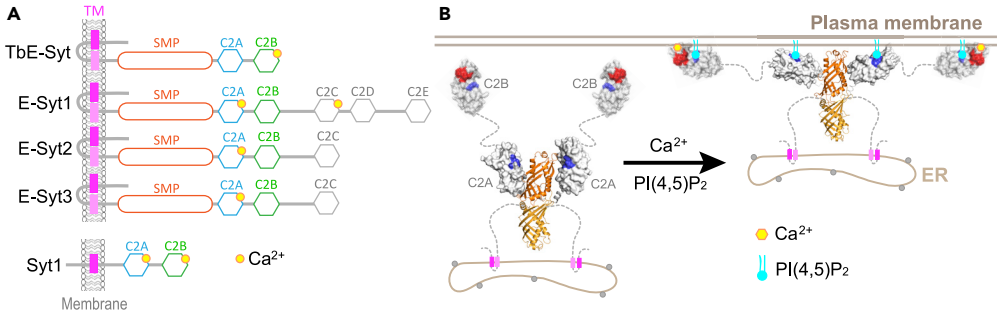

Figure 8. Structural comparison and hypothetical working model of TbE-Syt in lipid transferring

(A) Comparison of the domain arrangement of TbE-Syt and mammalian E-Syts and Syt1. All C2 domains in Syt1 bind Ca^{2+}, whereas only some of the C2 domains in the E-Syts bind Ca^{2+}. TbE-Syt is distinct from all known mammalian E-Syt1, 2, and 3 in that it contains only two C2 domains. Furthermore, TbE-Syt-C2B binds Ca^{2+} but TbE-Syt-C2A does not, which is the opposite of E-Syt1-3.

(B) Hypothetical model illustrating how the ER-anchored TbE-Syt might attach to the plasma membrane via both Ca^{2+}- and $PI(4,5)P_2$-mediated interactions. This would tether the cortical ER to the plasma membrane to allow the lipid-carrying SMP dimer to shuttle lipids between the two apposed membranes.

See also Figure S9.

at the distal tip of the newly assembled FAZ (Zhou et al., 2018). Therefore, under physiological conditions TbE-Syt likely localizes only to the FAZ-associated cortical ER apposed to the plasma membrane.

It was reported previously that inter-membrane lipid transfer by HsE-Syt2 is through its SMP domain as the carrier of phospholipids (Schauder et al., 2014). Homology modeling analyses showed that TbE-Syt-SMP has a similar deep hydrophobic cleft that could accommodate lipid molecules as in HsE-Syt2 (Figure 3). Similar to HsE-Syt2, the SMP of TbE-Syt could also form an end-to-end homodimer based on our bioinformatics analyses. Both the putative lipid-binding cleft in TbE-Syt-SMP and the hydrophobic dimeric interface are highly conserved in all trypanosome homologs, suggesting that TbE-Syt might employ a similar mechanism to carry and transfer lipids as that reported for HsE-Syt2.

We have determined a high-resolution crystal structure for the C-terminal C2 domain of TbE-Syt (Figure 4), which was designated as C2B based on its high structural similarity to HsE-Syt2-C2B (Figure S7). Our structure-based mutagenesis studies revealed that TbE-Syt-C2B bound lipids in both Ca^{2+}- and $PI(4,5)P_2$-dependent manners via an acidic patch and an extended basic patch, respectively (Figure 5). Although disruption of one site did not abolish lipid binding of the other, wild-type protein bound liposomes much more abundantly than either mutant that abolished one of the two binding sites. Therefore, the two sites seem to work cooperatively in lipid binding, similar to what was reported for C2 domains of Syt1 (Li et al., 2006; Radhakrishnan et al., 2009; van den Bogaart et al., 2012). For TbE-Syt-C2A, homology modeling suggested that it lacks nearly all acidic residues at the putative Ca^{2+} binding site. However, TbE-Syt-C2A retains a conserved basic patch similar to that on TbE-Syt-C2B (Figure 6). This suggests that TbE-Syt-C2A may use only the basic patch to interact with the negatively charged head groups of $PI(4,5)P_2$ enriched on the plasma membrane.

With only two C2 domains, TbE-Syt is the shortest E-Syt identified to date. This may correlate with the unique MCS between the FAZ-associated ER and the plasma membrane in *T. brucei*. The FAZ in trypanosomes forms an adhesion structure between the flagellar and the plasma membrane, with one portion of the FAZ filament tightly associated with the cortical ER (Lacomble et al., 2009; Vickerman, 1969). The specialized FAZ in trypanosomes makes the FAZ-associated ER in a close and constitutive contact with the plasma membrane. In such a case, a short tether like TbE-Syt would be sufficient to bridge the two apposed membranes to allow efficient lipid transfer between the FAZ-associated cortical ER and the plasma membrane. Furthermore, in contrast to other organisms, including yeast, plants, and animals, which all have several types of E-Syts, trypanosomes have only a single copy of E-Syt. This might also correlate with the specialized function of TbE-Syt at the MCS between the FAZ-associated ER and the plasma membrane in trypanosomes.

Based on the unique domain organization and distinct structure of TbE-Syt compared with mammalian E-Syts and Syt1 (Figure 8A), we propose a working model for how TbE-Syt might mediate lipid transfer

between the cortical ER and the plasma membrane in trypanosomes (Figure 8B). Two TbE-Syt molecules form a homodimer through the end-to-end interaction of their SMP domains. The C2A domain is connected to the SMP via a short linker (aa280–290), which is predicted to be ordered by ODiNPred (Figure S8A). Consistently, homology modeling based on the crystal structure of HsE-Syt-SMP-C2A (PDB: 4NPK) generated a compact structure of TbE-Syt-SMP-C2A (Figure S8B). To generate MCSs between the ER and the plasma membrane, the dimeric TbE-Syt is first anchored on the ER membrane via the N-terminal TM domains. The two C2B domains at the distal end of the structure would make initial contact with the plasma membrane both via the acidic patch in a Ca^{2+}-dependent manner and via the basic patch to interact with PI(4,5)P_2. It is noteworthy that the basic residues (K502, K511) in the PI(4,5)P_2-binding site on TbE-Syt-C2B are not as conserved as those acidic residues in the Ca^{2+}-binding site in other trypanosome species (Figure 1B), suggesting that the Ca^{2+}-binding site is the major and universal element for TbE-Syt-C2B to interact with the plasma membrane.

In contrast, the basic patch on TbE-Syt-C2A is highly conserved throughout all trypanosomes. Given that it lacks the Ca^{2+}-binding site, TbE-Syt-C2A would dock onto the plasma membrane solely in a PI(4,5)P_2-dependent fashion. Interestingly, the putative PI(4,5)P_2-binding site in the homologous model of TbE-Syt-C2A is orientated inward facing the tubular SMP (Figure 8B, left). In such case the hinge between the SMP and C2A domains would have to be partially opened to allow the exposure of the basic patch on the C2A domain to interact with the acidic head groups of PI(4,5)P_2 molecules on the plasma membrane. Notably, the linker connecting C2A and C2B contains a couple of conserved positively charged residues (Figure 1B), whereas high-throughput proteomics studies revealed six phosphorylation sites in this loop, i.e., S437, S441, S443, S447, S459, T460 (Alsford et al., 2011). These suggest that the linker between TbE-Syt-C2A and C2B may play a regulatory role in fine-tuning the interaction between TbE-Syt and the plasma membrane. Altogether, TbE-Syt could thereby tether and staple the FAZ-associated cortical ER onto the plasma membrane to allow the dimeric SMP domains, which could carry multiple lipid molecules in their hydrophobic clefts, to shuttle lipids originating from the ER membrane through their hydrophobic tunnels to the plasma membrane.

Limitations of the study

Although we have characterized the structure and membrane binding of the C2B domain of TbE-Syt, we could not express and purify its two other domains, i.e., SMP and C2A. This prevents us from revealing their atomic structures and carrying out lipid transfer assays as those previously reported for mammalian E-Syt2.

Resource availability

Lead contact

Further information and requests for resources and reagents should be directed to and will be fulfilled by the lead contact, Gang Dong (gang.dong@meduniwien.ac.at).

Materials availability

All unique/stable reagents generated in this study are available from the lead contact without restriction.

Data and code availability

The accession number for the crystal structure of TbE-Syt-C2B reported in this paper is PDB: 7A1R.

METHODS

All methods can be found in the accompanying transparent methods supplemental file.

SUPPLEMENTAL INFORMATION

Supplemental information can be found online at https://doi.org/10.1016/j.isci.2021.102422.

ACKNOWLEDGMENTS

We thank Drs. K. Ersfeld, J. Bangs, K. Gull, and P. Bastin for the antibodies of anti-myc, anti-BiP, L8C4, and L3B2, respectively. We also thank Dr. J. Sunter for sharing the raw imaging data of TbE-Syt that initially appeared on the TrypTag.org website. We are grateful to the staff at the beamline of ID23-2 at the European Synchrotron Radiation Facility (ESRF) for their help with X-ray diffraction, to Y. Zhang for generating the

TbE-Syt-YFP cells, and to W. Beatty (Washington University at St. Louis) for immuno-cryoEM. This work was supported by the grants P24383-B21, P28231-B28 and I4960-B from the Austrian Science Fund (FWF) to G.D., by the LabEx ParaFrap (ANR-11-LABX-0024) to D.R.R., by the CNRS and the University of Bordeaux to D.R.R. and M.B., and by grant MOE2017-T2-2-109 from the Singapore Ministry of Education to C.Y.H. E.S. was associated to the Integrative Structural Biology graduate program funded by the FWF (W-1258 Doktoratskollegs). We appreciate B. Morriswood for critical reading of the manuscript.

AUTHOR CONTRIBUTIONS

G.D. and D.R.R. conceived the project. J.L., D.S., and P.W. cloned the gene, expressed the proteins, and grew crystals. G.D. collected the diffraction data and carried out crystal structure determination and all bioinformatics analyses. E.S. and I.L. carried out liposome-binding assays. C.Y.H. coordinated immunofluorescence and immuno-EM analyses of TbE-Syt. N.L., D.R.R. and M.B. carried out all other *in vivo* analyses. G.D. wrote the manuscript with help of other authors.

DECLARATION OF INTERESTS

The authors declare no competing interests.

Received: March 8, 2021
Revised: April 3, 2021
Accepted: April 8, 2021
Published: May 21, 2021

REFERENCES

Aguilar, P.S., Engel, A., and Walter, P. (2007). The plasma membrane proteins Prm1 and Fig1 ascertain fidelity of membrane fusion during yeast mating. Mol. Biol. Cell *18*, 547–556.

Alsford, S., Turner, D.J., Obado, S.O., Sanchez-Flores, A., Glover, L., Berriman, M., Hertz-Fowler, C., and Horn, D. (2011). High-throughput phenotyping using parallel sequencing of RNA interference targets in the African trypanosome. Genome Res. *21*, 915–924.

Aslett, M., Aurrecoechea, C., Berriman, M., Brestelli, J., Brunk, B.P., Carrington, M., Depledge, D.P., Fischer, S., Gajria, B., Gao, X., et al. (2010). TriTrypDB: a functional genomic resource for the Trypanosomatidae. Nucleic Acids Res. *38*, D457–D462.

Bangs, J.D., Uyetake, L., Brickman, M.J., Balber, A.E., and Boothroyd, J.C. (1993). Molecular cloning and cellular localization of a BiP homologue in Trypanosoma brucei. Divergent ER retention signals in a lower eukaryote. J. Cell Sci. *105* (Pt 4), 1101–1113.

Beamer, L.J., Carroll, S.F., and Eisenberg, D. (1997). Crystal structure of human BPI and two bound phospholipids at 2.4 angstrom resolution. Science *276*, 1861–1864.

Bertoni, M., Kiefer, F., Biasini, M., Bordoli, L., and Schwede, T. (2017). Modeling protein quaternary structure of homo- and hetero-oligomers beyond binary interactions by homology. Sci. Rep. *7*, 10480.

Brose, N., Petrenko, A.G., Sudhof, T.C., and Jahn, R. (1992). Synaptotagmin: a calcium sensor on the synaptic vesicle surface. Science *256*, 1021–1025.

Chang, C.L., Hsieh, T.S., Yang, T.T., Rothberg, K.G., Azizoglu, D.B., Volk, E., Liao, J.C., and Liou, J. (2013). Feedback regulation of receptor-induced Ca2+ signaling mediated by E-Syt1 and Nir2 at endoplasmic reticulum-plasma membrane junctions. Cell Rep. *5*, 813–825.

Craxton, M. (2007). Evolutionary genomics of plant genes encoding N-terminal-TM-C2 domain proteins and the similar FAM62 genes and synaptotagmin genes of metazoans. BMC Genomics *8*, 259.

Dass, R., Mulder, F.A.A., and Nielsen, J.T. (2020). ODiNPred: comprehensive prediction of protein order and disorder. Sci. Rep. *10*, 14780.

Dean, S., Sunter, J.D., and Wheeler, R.J. (2017). TrypTag.org: a trypanosome genome-wide protein localisation resource. Trends Parasitol. *33*, 80–82.

Elferink, L.A., Peterson, M.R., and Scheller, R.H. (1993). A role for synaptotagmin (p65) in regulated exocytosis. Cell *72*, 153–159.

Fernandez-Busnadiego, R., Saheki, Y., and De Camilli, P. (2015). Three-dimensional architecture of extended synaptotagmin-mediated endoplasmic reticulum-plasma membrane contact sites. Proc. Natl. Acad. Sci. U S A *112*, E2004–E2013.

Gadelha, C., Wickstead, B., de Souza, W., Gull, K., and Cunha-e-Silva, N. (2005). Cryptic paraflagellar rod in endosymbiont-containing kinetoplastid protozoa. Eukaryot. Cell *4*, 516–525.

Giordano, F., Saheki, Y., Idevall-Hagren, O., Colombo, S.F., Pirruccello, M., Milosevic, I., Gracheva, E.O., Bagriantsev, S.N., Borgese, N., and De Camilli, P. (2013). PI(4,5)P(2)-dependent and Ca(2+)-regulated ER-PM interactions mediated by the extended synaptotagmins. Cell *153*, 1494–1509.

Guerrero-Valero, M., Ferrer-Orta, C., Querol-Audi, J., Marin-Vicente, C., Fita, I., Gomez-Fernandez, J.C., Verdaguer, N., and Corbalan-Garcia, S. (2009). Structural and mechanistic insights into the association of PKCalpha-C2 domain to PtdIns(4,5)P2. Proc. Natl. Acad. Sci. U S A *106*, 6603–6607.

Hayashi, M., Raimondi, A., O'Toole, E., Paradise, S., Collesi, C., Cremona, O., Ferguson, S.M., and De Camilli, P. (2008). Cell- and stimulus-dependent heterogeneity of synaptic vesicle endocytic recycling mechanisms revealed by studies of dynamin 1-null neurons. Proc. Natl. Acad. Sci. U S A *105*, 2175–2180.

Idevall-Hagren, O., Lu, A., Xie, B., and De Camilli, P. (2015). Triggered Ca2+ influx is required for extended synaptotagmin 1-induced ER-plasma membrane tethering. EMBO J. *34*, 2291–2305.

Kohl, L., Sherwin, T., and Gull, K. (1999). Assembly of the paraflagellar rod and the flagellum attachment zone complex during the Trypanosoma brucei cell cycle. J. Eukaryot. Microbiol. *46*, 105–109.

Kopec, K.O., Alva, V., and Lupas, A.N. (2011). Bioinformatics of the TULIP domain superfamily. Biochem. Soc. Trans. *39*, 1033–1038.

Lacomble, S., Vaughan, S., Gadelha, C., Morphew, M.K., Shaw, M.K., McIntosh, J.R., and Gull, K. (2009). Three-dimensional cellular architecture of the flagellar pocket and associated cytoskeleton in trypanosomes revealed by electron microscope tomography. J. Cell Sci. *122*, 1081–1090.

Lahiri, S., Toulmay, A., and Prinz, W.A. (2015). Membrane contact sites, gateways for lipid homeostasis. Curr. Opin. Cell Biol. *33*, 82–87.

Laskowski, R.A., and Swindells, M.B. (2011). LigPlot+: multiple ligand-protein interaction diagrams for drug discovery. J. Chem. Inf. Model. *51*, 2778–2786.

Levine, T., and Loewen, C. (2006). Inter-organelle membrane contact sites: through a glass, darkly. Curr. Opin. Cell Biol. *18*, 371–378.

Levy, A., Zheng, J.Y., and Lazarowitz, S.G. (2015). Synaptotagmin SYTA forms ER-plasma membrane junctions that are recruited to plasmodesmata for plant virus movement. Curr. Biol. *25*, 2018–2025.

Li, L., Shin, O.H., Rhee, J.S., Arac, D., Rah, J.C., Rizo, J., Sudhof, T., and Rosenmund, C. (2006). Phosphatidylinositol phosphates as co-activators of Ca2+ binding to C2 domains of synaptotagmin 1. J. Biol. Chem. *281*, 15845–15852.

Manford, A.G., Stefan, C.J., Yuan, H.L., Macgurn, J.A., and Emr, S.D. (2012). ER-to-plasma membrane tethering proteins regulate cell signaling and ER morphology. Dev. Cell *23*, 1129–1140.

McNicholas, S., Potterton, E., Wilson, K.S., and Noble, M.E. (2011). Presenting your structures: the CCP4mg molecular-graphics software. Acta Crystallogr. D Biol. Crystallogr. *67*, 386–394.

Min, S.W., Chang, W.P., and Sudhof, T.C. (2007). E-Syts, a family of membranous Ca2+-sensor proteins with multiple C2 domains. Proc. Natl. Acad. Sci. U S A *104*, 3823–3828.

Perin, M.S., Johnston, P.A., Ozcelik, T., Jahn, R., Francke, U., and Sudhof, T.C. (1991). Structural and functional conservation of synaptotagmin (p65) in Drosophila and humans. J. Biol. Chem. *266*, 615–622.

Qiu, X., Mistry, A., Ammirati, M.J., Chrunyk, B.A., Clark, R.W., Cong, Y., Culp, J.S., Danley, D.E., Freeman, T.B., Geoghegan, K.F., et al. (2007). Crystal structure of cholesteryl ester transfer protein reveals a long tunnel and four bound lipid molecules. Nat. Struct. Mol. Biol. *14*, 106–113.

Radhakrishnan, A., Stein, A., Jahn, R., and Fasshauer, D. (2009). The Ca2+ affinity of synaptotagmin 1 is markedly increased by a specific interaction of its C2B domain with phosphatidylinositol 4,5-bisphosphate. J. Biol. Chem. *284*, 25749–25760.

Saheki, Y., Bian, X., Schauder, C.M., Sawaki, Y., Surma, M.A., Klose, C., Pincet, F., Reinisch, K.M., and De Camilli, P. (2016). Control of plasma membrane lipid homeostasis by the extended synaptotagmins. Nat. Cell Biol. *18*, 504–515.

Schauder, C.M., Wu, X., Saheki, Y., Narayanaswamy, P., Torta, F., Wenk, M.R., De Camilli, P., and Reinisch, K.M. (2014). Structure of a lipid-bound extended synaptotagmin indicates a role in lipid transfer. Nature *510*, 552–555.

Sclip, A., Bacaj, T., Giam, L.R., and Sudhof, T.C. (2016). Extended synaptotagmin (ESyt) triple knock-out mice are viable and fertile without obvious endoplasmic reticulum dysfunction. PLoS One *11*, e0158295.

Sherwin, T., and Gull, K. (1989). The cell division cycle of Trypanosoma brucei brucei: timing of event markers and cytoskeletal modulations. Philos. Trans. R. Soc. Lond. B Biol. Sci. *323*, 573–588.

Simpson, A.G., Stevens, J.R., and Lukes, J. (2006). The evolution and diversity of kinetoplastid flagellates. Trends Parasitol. *22*, 168–174.

Toulmay, A., and Prinz, W.A. (2012). A conserved membrane-binding domain targets proteins to organelle contact sites. J. Cell Sci. *125*, 49–58.

Tremblay, M.G., and Moss, T. (2016). Loss of all 3 Extended Synaptotagmins does not affect normal mouse development, viability or fertility. Cell Cycle *15*, 2360–2366.

van den Bogaart, G., Meyenberg, K., Diederichsen, U., and Jahn, R. (2012). Phosphatidylinositol 4,5-bisphosphate increases Ca2+ affinity of synaptotagmin-1 by 40-fold. J. Biol. Chem. *287*, 16447–16453.

Vickerman, K. (1969). On the surface coat and flagellar adhesion in trypanosomes. J. Cell Sci. *5*, 163–193.

Waterhouse, A., Bertoni, M., Bienert, S., Studer, G., Tauriello, G., Gumienny, R., Heer, F.T., de Beer, T.A.P., Rempfer, C., Bordoli, L., et al. (2018). SWISS-MODEL: homology modelling of protein structures and complexes. Nucleic Acids Res. *46*, W296–W303.

Wong, L.H., and Levine, T.P. (2017). Tubular lipid binding proteins (TULIPs) growing everywhere. Biochim. Biophys. Acta Mol. Cell Res. *1864*, 1439–1449.

Xu, J., Bacaj, T., Zhou, A., Tomchick, D.R., Sudhof, T.C., and Rizo, J. (2014). Structure and Ca(2)(+)-binding properties of the tandem C(2) domains of E-Syt2. Structure *22*, 269–280.

Zhou, Q., An, T., Pham, K.T.M., Hu, H., and Li, Z. (2018). The CIF1 protein is a master orchestrator of trypanosome cytokinesis that recruits several cytokinesis regulators to the cytokinesis initiation site. J. Biol. Chem. *293*, 16177–16192.

iScience, Volume *24*

Supplemental information

Structural studies of the shortest extended synaptotagmin with only two C2 domains from *Trypanosoma brucei*

Emma Stepinac, Nicolas Landrein, Daria Skwarzyńska, Patrycja Wójcik, Johannes Lesigang, Iva Lučić, Cynthia Y. He, Mélanie Bonhivers, Derrick R. Robinson, and Gang Dong

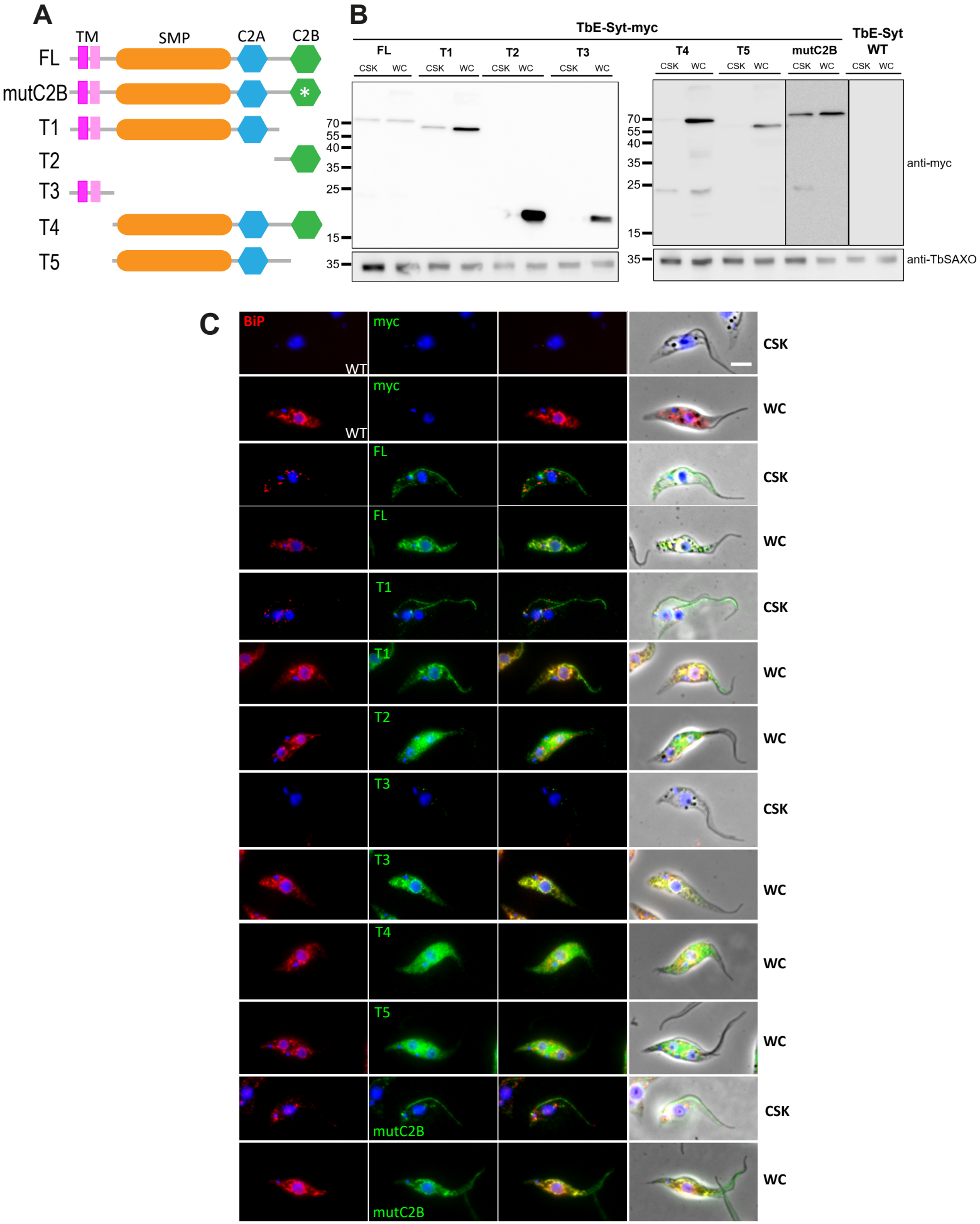

6-24h induction with 10ng/ml tetracycline (T3 with 100ng/ml)

CSK: cytoskeleton extracted cells; **WC:** whole cells

Figure S1. Localization of TbE-Syt at the ER. Related to Figure 2. (**A**) Schematic representations of the C-terminally myc-tagged TbE-Syt constructs, including full-length (FL), mutC2B (E492A/D498A), and five truncations (T1-T5), expressed in procyclic form *T. brucei*. (**B**) Western blot analysis of the level of expression of TbE-Syt-myc constructs in whole cells (WC) and their association with the cytoskeleton in detergent-extracted cells (CSK). Anti-TbSAXO antibodies were used as a loading control. (**C**) Labeling of BiP and myc-tagged TbE-Syt, mutC2B, and truncations T1-T5 in whole cells (WC) and cytoskeletons (CSK). The kinetoplasts and nuclei were stained with DAPI. Scale bar, 5 μm.

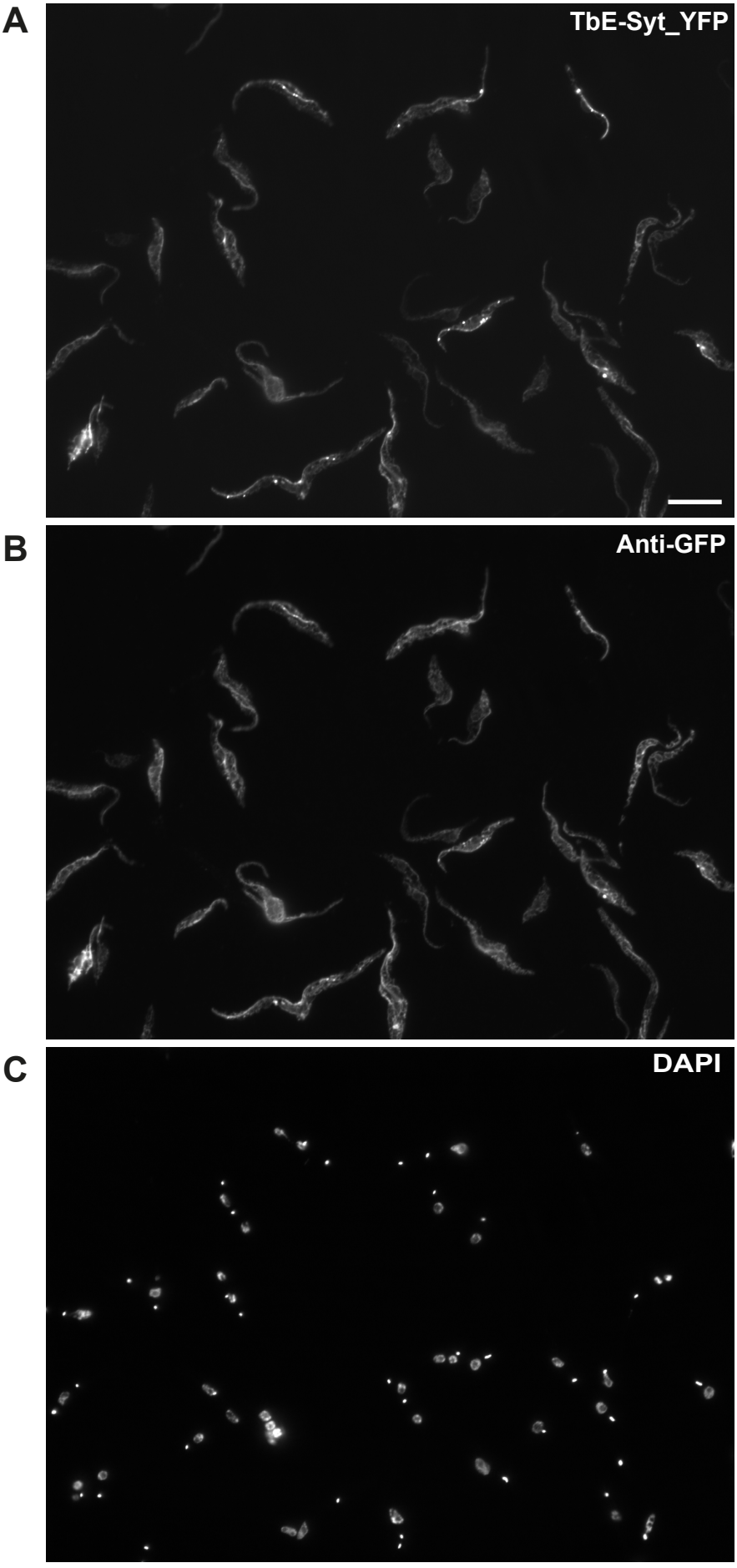

Figure S2. TbE-Syt-YFP localized to both the FAZ-associated ER and the central ER. Related to Figure 2. Note: YFP fluorescence (A) gave slightly weaker but sharper signals than anti-GFP immunofluorescence (B). Scale bar, 10 μm.

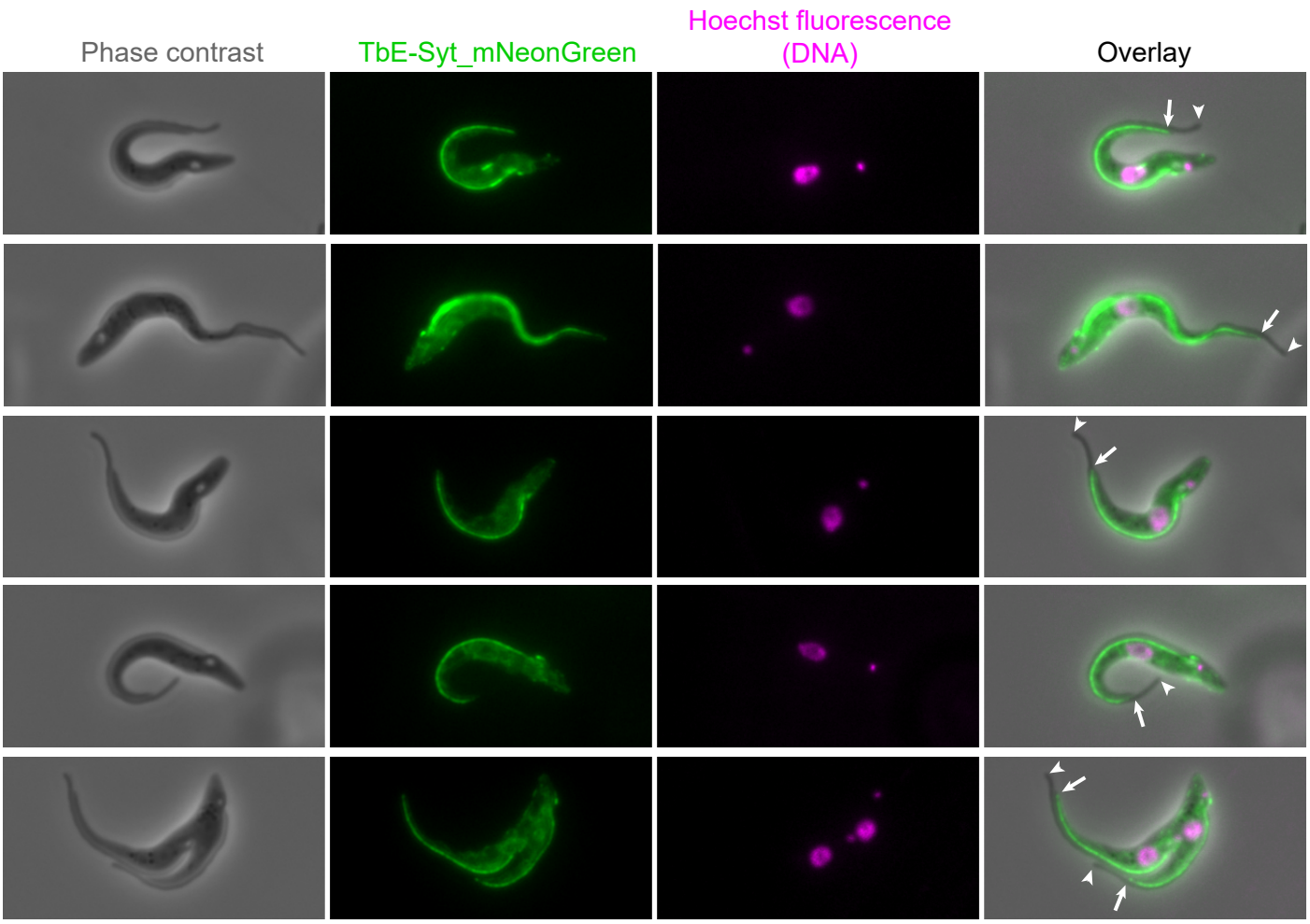

Figure S3. Location of TbE-Syt in procyclic form *T. brucei* reported in the TrypTag database
Related to Figure 2. Five images with cells expressing TbE-Syt-mNeonGreen were imaged with phase contrast, mNeonGreen fluorescence, and Hoechst 33342 fluorescence. Hoechst 33342 is a fluorescent marker for DNA in the nucleus and kinetoplast (Hoechst). In the overlaid images on the right, the flagellar tips and the tips of the FAZ are marked by arrowheads and arrows, respectively. Images taken with permission from the TrypTag database (http://tryptag.org).

A

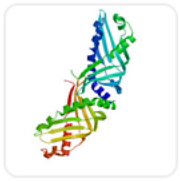

Model 01

Structure Assessment

Oligo-State
Homo-dimer (matching prediction)

Ligands
None

GMQE
0.65

QMEAN
-3.32

Global Quality Estimate

QMEAN	-3.32
Cβ	-2.06
All Atom	-1.37
solvation	0.09
torsion	-3.05

Local Quality Estimate

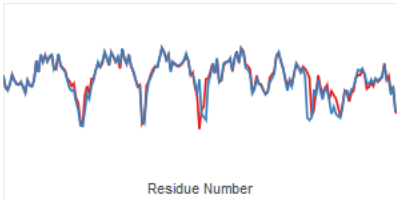

Comparison

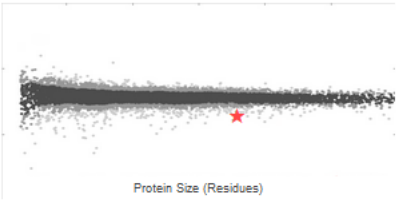

Template	Seq Identity	Coverage	Description
4p42.1.A	20.45%		Extended synaptotagmin-2

Model-Template Alignment

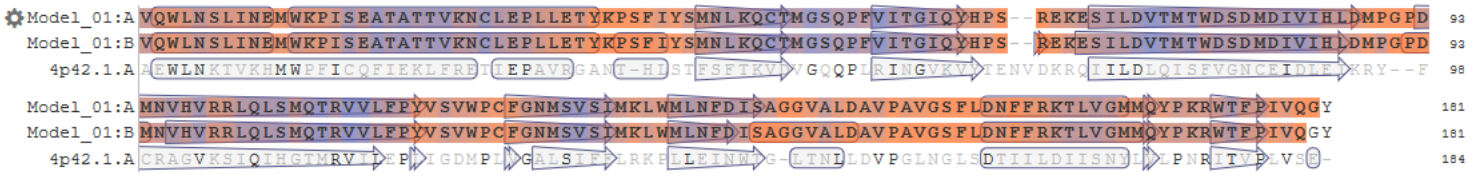

B

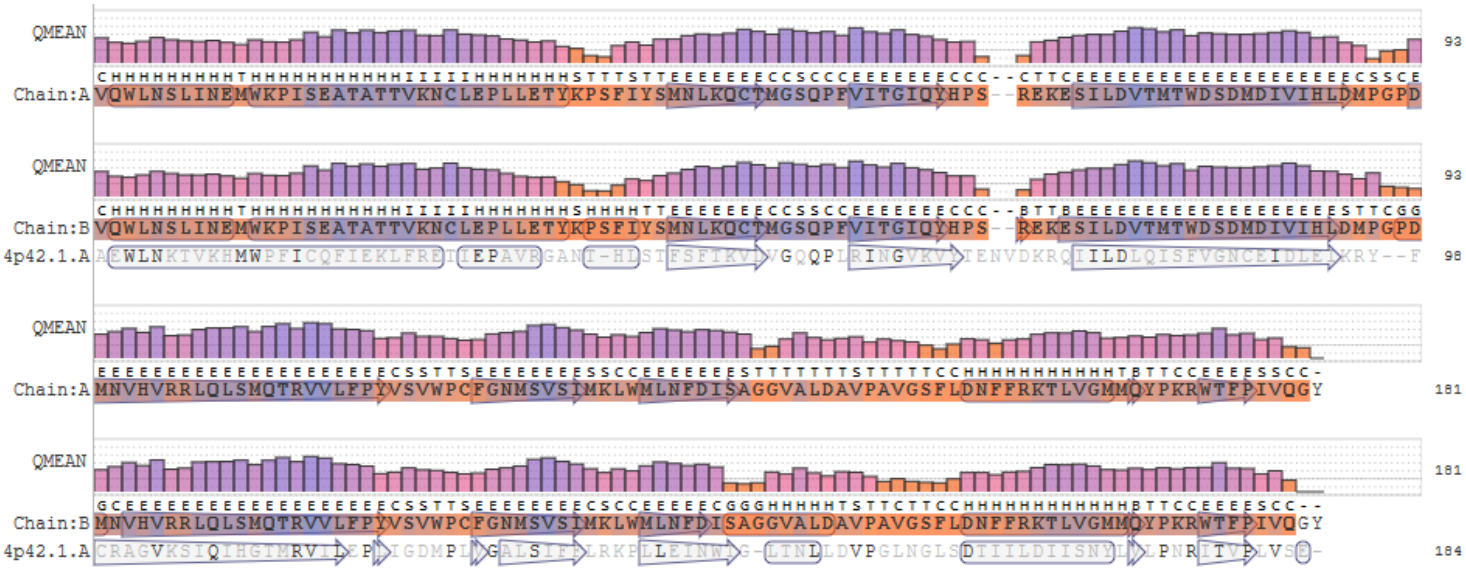

C

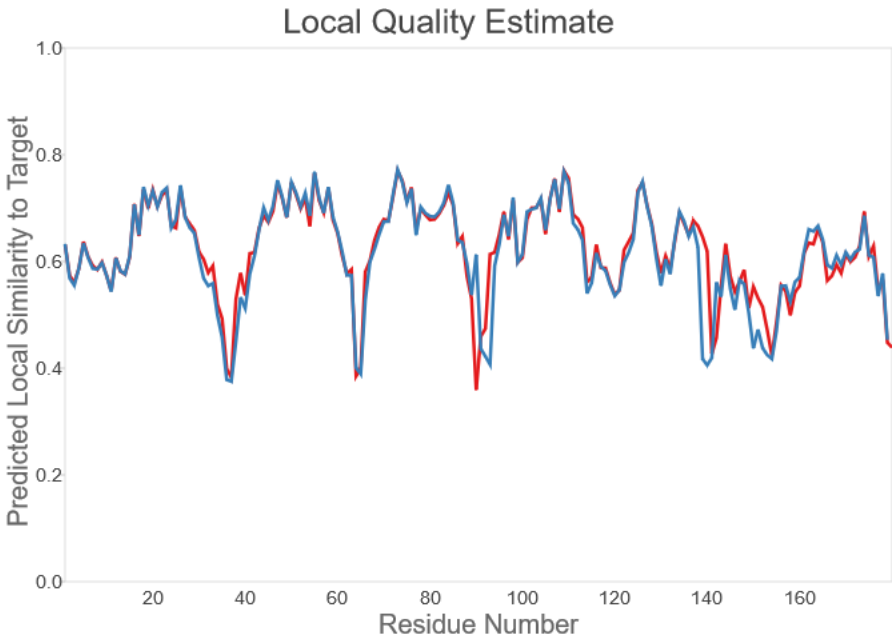

Figure S4. Homology modeling of the TbE-Syt-SMP dimer. Related to Figure 3. (**A**) Homology modeling of TbE-Syt-SMP by SWISS-MODEL using the HsE-Syt2-SMP structure (4P42.pdb) as the template. (**B**) Alignment of chains A and B of the homodimeric TbE-Syt-SMP model along the template with secondary structures shown in the DSSP mode and individual residues colored based on QMEAN values. (**C**) Local quality estimate for each residue in the final model. The two monomers are colored in red and blue.

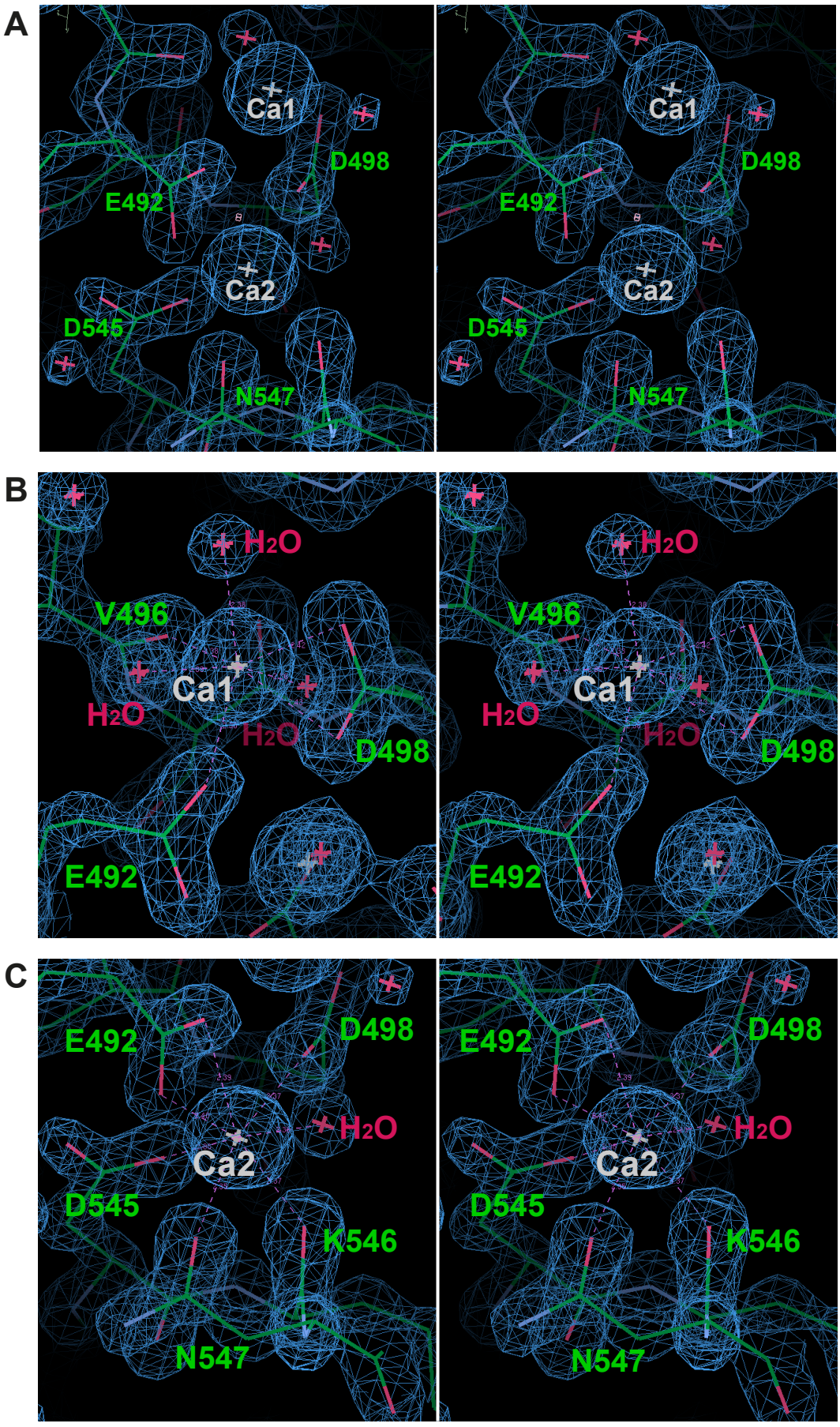

Figure S5. Electron density maps of TbE-Syt-C2B around the two Ca^{2+}-binding sites. Related to Figure 4. Stereo views of the $2F_o$-F_c maps around both (**A**) or each (**B** & **C**) of the two Ca^{2+}-binding sites. The maps were contoured at 2 σ level. Amino acids and water molecules hydrogen-bonded to the two Ca^{2+} ions are labeled in green and red, respectively.

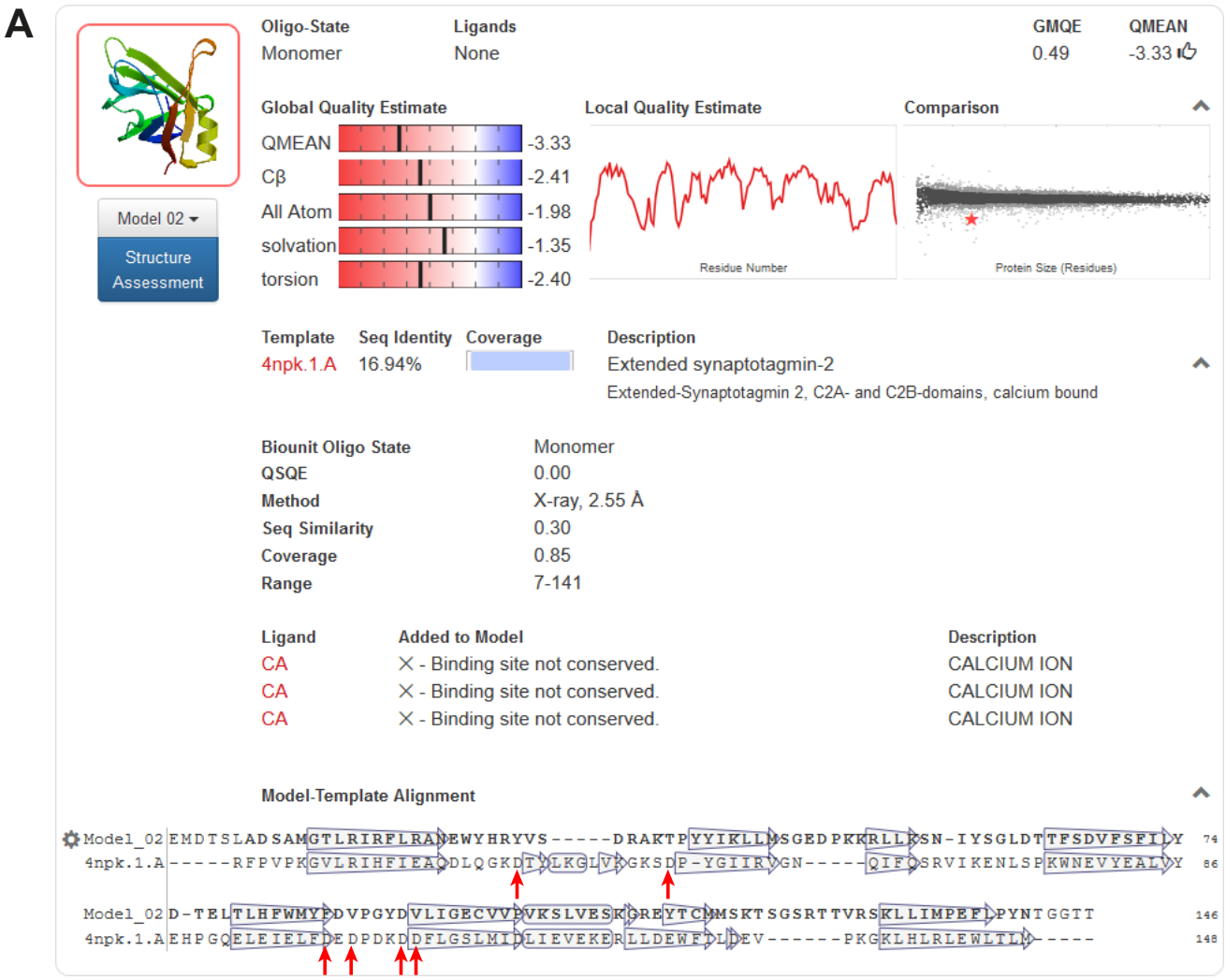
A
Oligo-State
Monomer
Ligands
None
GMQE
0.49
QMEAN
-3.33
Global Quality Estimate
QMEAN -3.33
Cβ -2.41
All Atom -1.98
solvation -1.35
torsion -2.40
Local Quality Estimate
Residue Number
Comparison
Protein Size (Residues)
Model 02
Structure Assessment
Template
4npk.1.A
Seq Identity
16.94%
Coverage
Description
Extended synaptotagmin-2
Extended-Synaptotagmin 2, C2A- and C2B-domains, calcium bound
Biounit Oligo State Monomer
QSQE 0.00
Method X-ray, 2.55 Å
Seq Similarity 0.30
Coverage 0.85
Range 7-141
Ligand
Added to Model
Description
CA ✕ - Binding site not conserved. CALCIUM ION
CA ✕ - Binding site not conserved. CALCIUM ION
CA ✕ - Binding site not conserved. CALCIUM ION
Model-Template Alignment
Model_02
4npk.1.A

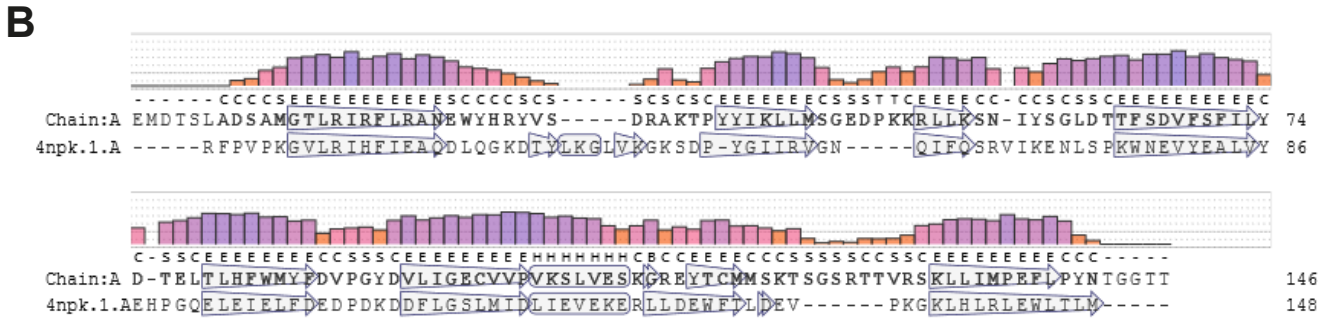
B
Chain:A
4npk.1.A

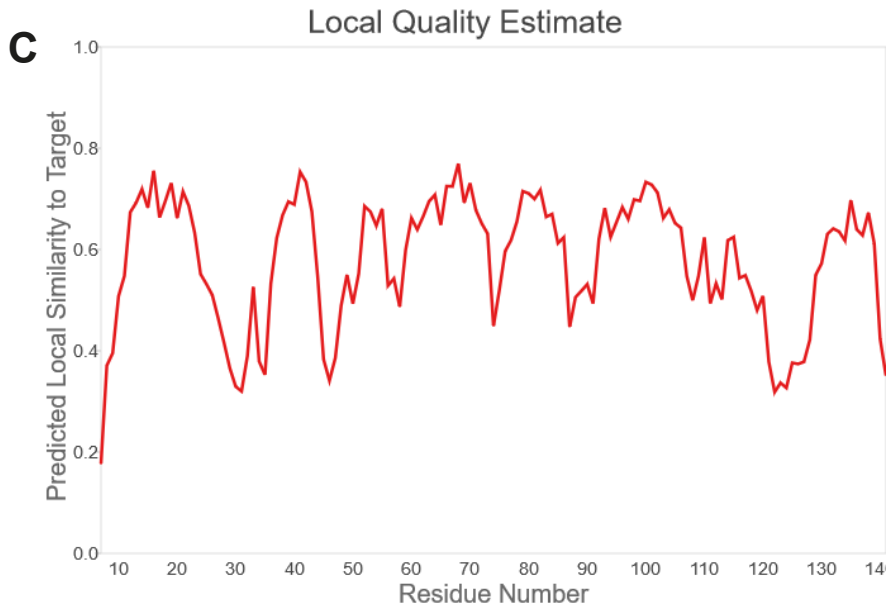
C
Local Quality Estimate
Predicted Local Similarity to Target
Residue Number

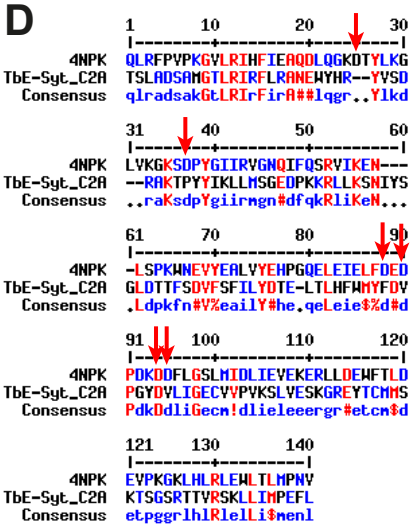
D
4NPK
TbE-Syt_C2A
Consensus

Figure S6. Homology modeling of TbE-Syt-C2A. Related to Figure 6. (**A**) Homology modeling of TbE-Syt-C2A by SWISS-MODEL using the HsE-Syt2-C2A structure (4NPK.pdb) as the template. Note that the three Ca^{2+}-binding sites, which are marked by arrows in the template, are not conserved in TbE-Syt-C2A. (**B**) Alignment of the TbE-Syt-C2A model with the template with secondary structures shown in the DSSP mode. (**C**) Local quality estimate for each residue in the final model. (**D**) Sequence alignment of HsE-Syt2-C2A (4NPK) and TbE-Syt-C2A using the hierarchical clustering based multiple sequence alignment tool MultAlin (http://multalin.toulouse.inra.fr/multalin/). Marked by arrows are the residues coordinating Ca^{2+} binding in HsE-Syt2-C2A. This further confirms that the absence of negatively residues at the putative Ca^{2+}-binding sites in TbE-Syt-C2A.

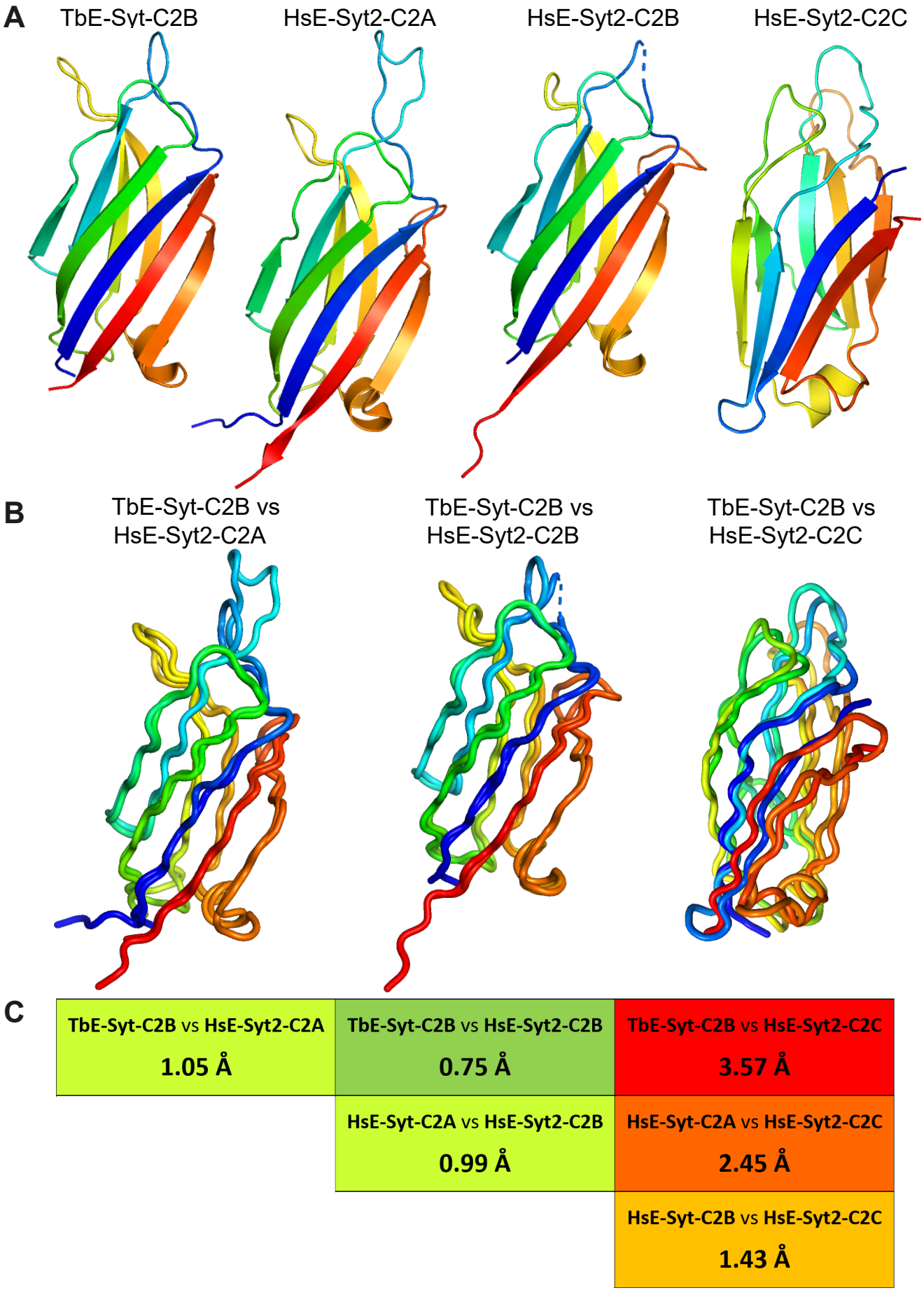

Figure S7. Structural comparison of TbE-Syt-C2B with the three C2 domains of HsE-Syt2. Related to Figure 7. (**A**) Ribbon diagrams of TbE-Syt-C2B and HsE-Syt2-C2A, C2B and C2C. All structures are rainbow colored from blue (N-terminus) to red (C-terminus). (**B**) TbE-Syt-C2B superimposed onto HsE-Syt2-C2A, C2B and C2C. (**C**) R.M.S.D values for each pair of superimposed structures.

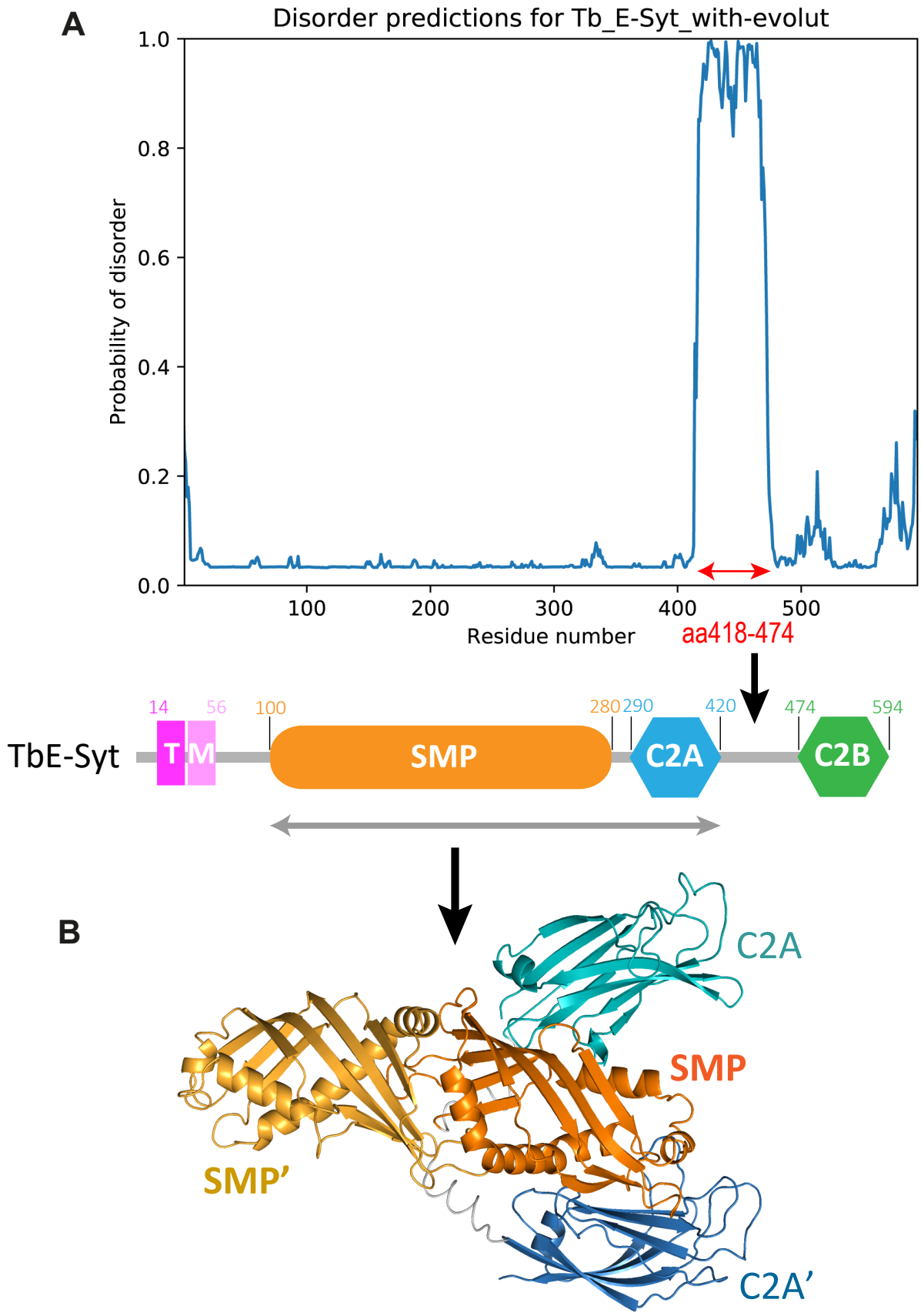

Figure S8. Folding and structure prediction of TbE-Syt. Related to Figure 7. (**A**) Disorder predictions of TbE-Syt by ODiNPred. Residues 418-474 of TbE-Syt was predicted to have very high probabilities of being disordered, which is consistent with the low conservation and variable lengths of this connecting loop in different homologs of TbE-Syt (see Fig. 1B). (**B**) Homology model of TbE-Syt-SMP-C2A (aa97-420) generated by SWISS-MODEL using the crystal structure of HsE-Syt2 (4NPK.pdb) as the template. The short linker (aa280-290) between the SMP and C2A domains, which are colored grey, suggests a relatively tight packing between these two domains. This is supported by predicted low disorder probability of this region (A) and is consistent with the structure of the counterpart in HsE-Syt2.

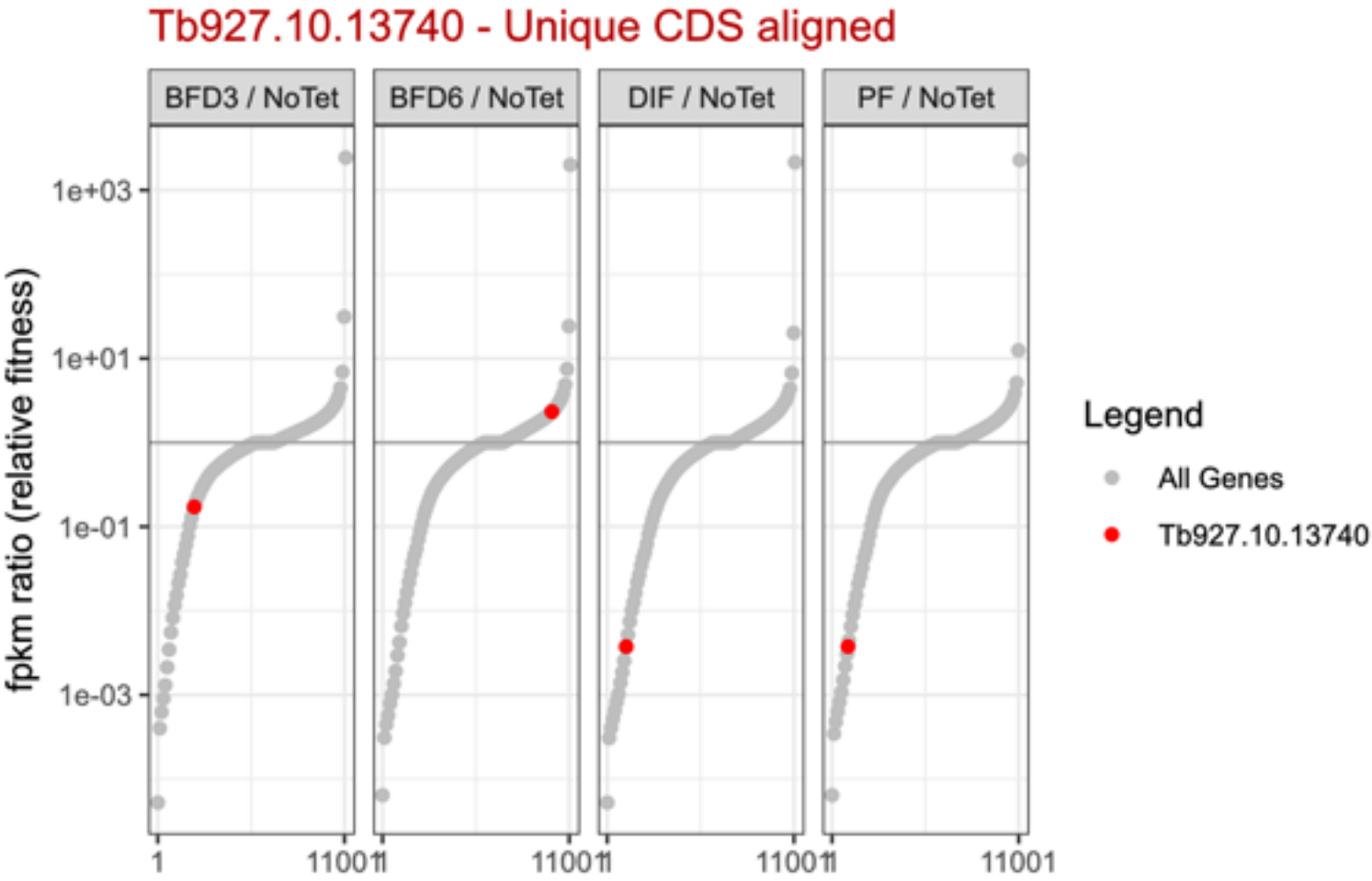

https://tritrypdb.org/tritrypdb/app/record/gene/Tb927.10.13740

Figure S9. Phenotypes of High-throughput TbE-Syt RNAi in *T. brucei* reported in the TriTrypDB database. Related to Figure 8. There was a very mild effect in the bloodstream form three (BFD3) and six days (BFD6) post RNAi induction. However, a strong negative score was recorded in the procyclic form, whether RNAi was induced in the procyclic form (PF) or during differentiation (DIF), which suggests that the protein is essential for cell viability of procyclic form *T. brucei*. Data copied with permission from TriTrypDB (http://tritrypdb.org).

Transparent Methods

Cloning and site-directed mutagenesis

For *in vivo* assays, the TbE-Syt ORF (Tb927.10.13740) was amplified by PCR from *T. brucei* TREU927/4 GUTat10.1 genomic DNA (Berriman et al., 2005) and cloned into modified pLew100 vector containing the puromycin resistance gene (Wirtz et al., 1999). This allowed tetracycline-inducible expression of 3xmyc C-terminal tagged TbE-Syt and various trucations (ΔC2B: aa1-473; C2B: aa474-594; TM: aa1-96; ΔTM: aa97-594; C2A-SMP: aa97-473). The mutant E492A/D498A (mutC2B) was generated in pLew100-TbE-Syt-myc subsequently by site-directed mutagenesis using a QuikChange kit (Stratagene) according to the manufacturer's instructions. For the RNAi experiments in procyclic form and bloodstream form, a *TbE-Syt* fragment (bp 957-1581) was cloned into the double promoter p2T7^{TiB}-GFP vector (LaCount et al., 2002), and the pLew100 for stem-loop construct (Wirtz et al., 1999). All cloned constructs were verified by DNA sequencing.

For bacterial purification, full-length TbE-Syt (aa1-594) was amplified by PCR from the *T. brucei* genomic DNA and ligated into the expression vector pET15b (Novagen) between the *Nde*I and *BamH*I sites. Various truncations of TbE-Syt, including TM-SMP-C2A-C2B (aa60-594), TM-SMP-C2A (aa60-422), TM-SMP (aa60-285), SMP-C2A-C2B (aa94-594), SMP-C2A (aa94-422), SMP (aa94-285), C2A-C2B (aa282-594), C2A (aa282-422), and C2B (aa459-594), were subcloned from the full-length construct into both pET15b (Novagen) and a custom vector MalpET that provides a fusion tag of maltose-binding protein (MBP) to the N-terminus of the truncated fragments. However, except for the construct of C2B (aa459-594), none of the other truncations yielded soluble proteins.

TbE-Syt-C2B (aa459-594) cloned into pET15b yielded protein with an N-terminal His_6 tag that was cleavable by thrombin. The three mutants, E492A/D498A, K502E/K511E and E492A/D498A/K502E/K511E, were subsequently generated based on this construct by site-directed mutagenesis using the QuikChange kit (Stratagene) according to the manufacturer's instructions. Incorporations of mutations were confirmed by DNA sequencing.

Trypanosome cell lines, growth conditions and transfection

The TbE-Syt ORF (Tb927.10.13740) was amplified by PCR from genomic DNA of *T. brucei* TREU927/4 GUTat10.1 (Melville et al., 2000). The trypanosome cell lines *T. brucei* 427 procyclic form 29-13 and bloodstream form 90-13 co-expressing the T7 RNA polymerase and tetracycline repressor (Wirtz et al., 1999) were grown and transfected as described before (Pradel et al., 2006). After transfection, the cells were selected with puromycin (1 µg/ml) and phleomycin 5 µg/ml (procyclic form) and 2.5 µg/ml (bloodstream form) as appropriate. Clones were selected after serial dilutions. Ectopic expression and

RNAi were induced with tetracycline at 10 ng/ml (except TbE-Syt TM$_{::myc}$ expression that was induced at 100 ng/ml) and 1-10 µg/ml, respectively.

Protein expression and purification

Recombinant His$_6$-TbE-Syt-C2B and the three mutants were expressed in the *E. coli* strain BL21(DE3). The bacterial cells transformed with individual constructs were grown in Luria-Bertani (LB) medium at 37°C with continuous agitation to an OD_{600} of 0.6-0.8, and then placed on ice for 30 min (cold shock). Induction of protein expression was done by addition of 0.5 mM isopropyl β-D-1-thiogalactopyranoside (IPTG), and the cells were further incubated at 16°C overnight (14-16 h) with continuous agitation. Bacterial cells were harvested by centrifugation in a Sorvall GS3 rotor (6,000×g, 12 min, 4°C), and the pellet was resuspended in 20 ml of lysis buffer (20 mM Tris-HCl pH 8.0, 100 mM NaCl, 20 mM imidazole, 5% (v/v) glycerol) per liter of cell culture.

Harvested cells were lysed in an EmulsiFlex-C3 homogenizer (Avestin) and cell debris was removed by centrifugation (40,000×g, 40 min, 4°C). The resulting supernatant was filtered (0.45-µm, Amicon) and loaded onto a 5-ml Ni-HiTrap column (GE Healthcare) that was pre-equilibrated with the same lysis buffer. The column was washed with 5 × column volume (cv) of lysis buffer, and bound protein was subsequently eluted using a linear gradient concentration of imidazole (20 - 500 mM, 20×cv) in the same lysis buffer.

The N-terminal His$_6$ tag was removed by incubating the pooled fractions containing wild-type or mutant TbE-Syt-C2B with ~2% (w/w) of thrombin (4°C, overnight). Target proteins were further purified on a Superdex-200 16/60 column (GE Healthcare), which was pre-equilibrated with buffer containing 20 mM Tris-HCl (pH 8.0) and 100 mM NaCl. The eluted proteins were pooled and concentrated using the centrifugal filters (MWCO 3,000, Amicon), and protein concentration was determined using ultraviolet (UV) absorbance at 280 nm and double-checked on SDS-PAGE gels for quality control.

Se-Met-substituted TbE-Syt-C2B was expressed following previously reported protocols (Doublie, 1997). Purification was carried out using the same protocol as for the wild-type protein, except that 15 mM β-mercaptoethanol and 10 mM DTT was added to the lysis buffer and the gel filtration buffer, respectively. The purified protein was concentrated to ~15 mg/ml for crystallization trials.

Crystallization, data collection and structure determination

Small clustered crystals of TbE-Syt-C2B were originally obtained in a large-scale crystallization screening trial using native protein and commercial crystallization screening kits (Hampton Research). Rod-shaped crystals of Se-Met-substituted TbE-Syt-C2B were subsequently obtained upon extensive optimization tests. The final crystallization conditions contained 0.1 M sodium cacodylate (pH 6.5), 0.15 M sodium acetate, and 28%

(v/v) polyethylene glycol 8,000. Crystals were harvested by sequentially soaking in the same reservoir solution with 5%, 10% and 15% (v/v) glycerol, loop mounted, and then flash frozen in liquid nitrogen. Diffraction data were collected at the beamline ID23-2 of the European Synchrotron Radiation Facility (ESRF), which ran at the fixed wavelength of 0.873 Å (14.2 keV). To minimize radiation damage, the data used for final structure determination were collected using the helical data acquisition mode to scan along the long axis of the crystal rod. All data were integrated and scaled using XDS (Kabsch, 2010).

Structure determination was carried out using the single-wavelength anomalous diffraction method. Selenium sites were located and experimental electron density maps calculated using the program AutoSol within the Phenix suite (Terwilliger et al., 2009). Partially built models were checked and missing loops were manually added in COOT (Emsley and Cowtan, 2004). Refinement was done using phenix.refine (Afonine et al., 2012).

Liposome pelleting assay with sucrose-loaded vesicles

Sucrose-loaded vesicles were prepared as follows: all lipids were reconstituted in chloroform and mixed in molar ratio of 20% cholesterol, 15% DOPS, 35% DOPE, and 30% DOPC, with 60 µM rhodamine dye. PI(4,5)P_2-containing vesicles had 5% of PI(4,5)P_2 and 25% of DOPC. The lipid mixture was dried to a thin film under weak nitrogen stream, hydrated in 20 mM HEPES (pH 7.5), 0.3 M sucrose and vortexed vigorously for 1 min at RT. The multilamellar vesicles created by this process were then subjected to four cycles of freezing in liquid nitrogen followed by thawing in a sonicating water bath at RT. This mixture of small unilamellar vesicles was diluted with 20 mM HEPES (pH 7.5), 100 mM KCl and pelleted at 230,000 × g for 30 min at RT. The pelleted vesicles were resuspended in 20 mM HEPES (pH 7.5), 100 mM KCl and incubated with purified protein at a 1:1 ratio for 30 min at RT. For Ca^{2+}-mediated liposome binding tests, proteins were incubated with 2 mM $CaCl_2$ for 5 min at RT prior to mixing with the vesicles. To separate soluble and sucrose-loaded vesicles-bound proteins, the mixtures were pelleted at 8000 × g for 30 min at RT, and equal volumes of supernatant and resuspended pellets were analyzed on SDS-PAGE gels.

Western blotting

Cells (2×10^7) were split for whole cells (WC) and cytoskeleton (CSK) samples and processed for western blotting analysis as described before (Florimond et al., 2015). Briefly, protein samples (equivalent to 5×10^6 trypanosomes whole cell or cytoskeletons) were separated on 15% (w/v) SDS-PAGE gels and transferred by semi-dry (BioRad) blotting to PVDF membranes. After blocking, the membranes were incubated overnight at 4°C with the anti-myc (9E10 mouse monoclonal, 1:10,000) primary antibody. After washes in 1 M NaCl and in blocking solution, the membranes were incubated for 1 h at RT with

the secondary antibody [anti-mouse HRP-conjugated (Jackson, 1:10,000)]. Blots were visualized using the Clarity Western ECL Substrate kit (Bio-Rad) on an ImageQuant LAS4000. After stripping in 100 mM glycine (pH 2.3), 0.1% (v/v) IGEPAL CA-630 and 1% (w/v) SDS, the membranes were processed as above with anti-TbSAXO (mAb25) antibodies as a loading control (Dacheux et al., 2012).

Immunofluorescence and microscopy

Wide-field fluorescence microscopy on *T. brucei* cells were processed for whole cell (WC) or detergent-extracted cytoskeletons (CSK) immunolabeling as described before (Florimond et al., 2015). Briefly, the slides were incubated with primary antibodies [anti-BiP (Bangs et al., 1993) 1:4,000, anti-myc (monoclonal 9E10) 1:20, L8C4 neat, and L3B2 1:25] and washed 2 x 5 min in PBS, then incubated with the secondary antibodies [anti-rabbit Alexa594-conjugated (Fischer A11012) 1:100; anti-mouse FITC-conjugated (Sigma F-2012)]. After DAPI staining (5 min, 10 µg/ml in PBS), the slides were mounted with SlowFAde Gold Antifade reagent. Images were acquired on a Zeiss Imager Z1 microscope with a Zeiss 100x objective (NA 1.4), using a Photometrics Coolsnap HQ2 camera and Metamorph software (Molecular Devices), and processed with ImageJ. Pearson's correlation coefficients were calculated (n = 22) for the TbE-Syst constructs FL, T1, T3, and mutC2B using the imageJ JaCoP plugin (Bolte and Cordelieres, 2006) and Costes's randomization (Costes et al., 2004). The large cytosolic pool of T4 and T2 prevented the analysis.

Immuno-cryoEM was performed by Dr. Wandy Beatty (Washington University) as described previously (Zhou et al., 2011). Briefly, cells stably expressing TbE-Syt-YFP were fixed with 4% (w/v) paraformaldehyde solution and 0.2% (w/v) glutaraldehyde (EMS) in 100 mM phosphate buffer (pH 7.2) for 1 h at 4°C. The fixed cells were embedded in 10% gelatin and infiltrated with 2.3 M sucrose, 20% polyvinyl pyrrolidone in PIPES-NaOH (pH 6.9) containing 1 mM $MgCl_2$. Liquid nitrogen frozen sections were obtained using a Leica Ultracut UCT cryoultramicrotome (Leica Microsystems, Bannockburn, IL), and processed for immunolabeling with anti-GFP antibodies (Abcam, UK), followed with secondary antibodies conjugated to colloidal gold (Jackson ImmunoResearch Laboratories). Labeled sections were visualized with a JEOL 1200 EX electron microscope (JEOL).

Supplemental References

Afonine, P.V., Grosse-Kunstleve, R.W., Echols, N., Headd, J.J., Moriarty, N.W., Mustyakimov, M., Terwilliger, T.C., Urzhumtsev, A., Zwart, P.H., and Adams, P.D. (2012). Towards automated crystallographic structure refinement with phenix.refine. Acta Crystallogr D Biol Crystallogr *68*, 352-367.

Bangs, J.D., Uyetake, L., Brickman, M.J., Balber, A.E., and Boothroyd, J.C. (1993). Molecular cloning and cellular localization of a BiP homologue in Trypanosoma brucei. Divergent ER retention signals in a lower eukaryote. J Cell Sci *105 (Pt 4)*, 1101-1113.

Berriman, M., Ghedin, E., Hertz-Fowler, C., Blandin, G., Renauld, H., Bartholomeu, D.C., Lennard, N.J., Caler, E., Hamlin, N.E., Haas, B.*, et al.* (2005). The genome of the African trypanosome Trypanosoma brucei. Science *309*, 416-422.

Bolte, S., and Cordelieres, F.P. (2006). A guided tour into subcellular colocalization analysis in light microscopy. J Microsc *224*, 213-232.

Costes, S.V., Daelemans, D., Cho, E.H., Dobbin, Z., Pavlakis, G., and Lockett, S. (2004). Automatic and quantitative measurement of protein-protein colocalization in live cells. Biophys J *86*, 3993-4003.

Dacheux, D., Landrein, N., Thonnus, M., Gilbert, G., Sahin, A., Wodrich, H., Robinson, D.R., and Bonhivers, M. (2012). A MAP6-related protein is present in protozoa and is involved in flagellum motility. PLoS One *7*, e31344.

Doublie, S. (1997). Preparation of selenomethionyl proteins for phase determination. Methods Enzymol *276*, 523-530.

Emsley, P., and Cowtan, K. (2004). Coot: model-building tools for molecular graphics. Acta Crystallogr D Biol Crystallogr *60*, 2126-2132.

Florimond, C., Sahin, A., Vidilaseris, K., Dong, G., Landrein, N., Dacheux, D., Albisetti, A., Byard, E.H., Bonhivers, M., and Robinson, D.R. (2015). BILBO1 is a scaffold protein of the flagellar pocket collar in the pathogen Trypanosoma brucei. PLoS Pathog *11*, e1004654.

Kabsch, W. (2010). Xds. Acta Crystallogr D Biol Crystallogr *66*, 125-132.

LaCount, D.J., Barrett, B., and Donelson, J.E. (2002). Trypanosoma brucei FLA1 is required for flagellum attachment and cytokinesis. J Biol Chem *277*, 17580-17588.

Melville, S.E., Leech, V., Navarro, M., and Cross, G.A. (2000). The molecular karyotype of the megabase chromosomes of Trypanosoma brucei stock 427. Mol Biochem Parasitol *111*, 261-273.

Pradel, L.C., Bonhivers, M., Landrein, N., and Robinson, D.R. (2006). NIMA-related kinase TbNRKC is involved in basal body separation in Trypanosoma brucei. J Cell Sci *119*, 1852-1863.

Terwilliger, T.C., Adams, P.D., Read, R.J., McCoy, A.J., Moriarty, N.W., Grosse-Kunstleve, R.W., Afonine, P.V., Zwart, P.H., and Hung, L.W. (2009). Decision-making in structure solution using Bayesian estimates of map quality: the PHENIX AutoSol wizard. Acta Crystallogr D Biol Crystallogr *65*, 582-601.

Wirtz, E., Leal, S., Ochatt, C., and Cross, G.A. (1999). A tightly regulated inducible expression system for conditional gene knock-outs and dominant-negative genetics in Trypanosoma brucei. Mol Biochem Parasitol *99*, 89-101.

Zhou, Q., Liu, B., Sun, Y., and He, C.Y. (2011). A coiled-coil- and C2-domain-containing protein is required for FAZ assembly and cell morphology in Trypanosoma brucei. J Cell Sci *124*, 3848-3858.

KEY RESOURCES TABLE

REAGENT or RESOURCE	SOURCE	IDENTIFIER
Antibodies		
Anti-GFP	Abcam	ab6556
Anti-PFR	Zhang et al., 2018	https://jcs.biologists.org/content/131/17/jcs219071
L3B2	Kohl et al., 1999	https://onlinelibrary.wiley.com/doi/abs/10.1111/j.1550-7408.1999.tb04592.x
Anti myc clone 9E10	K. Ersfeld	N/A
Anti BiP	Bangs et al., 1993	https://jcs.biologists.org/content/105/4/1101
Anti-TbSAXO	Dacheux et al., 2012	https://doi.org/10.1371/journal.pone.0031344"
Anti-PFR L8C4	Kohl et al., 1999	https://doi.org/10.1111/j.1550-7408.1999.tb04592.x
Bacterial and virus strains		
E. coli BL21(DE3)	Novagen	Cat#69450
E. coli HST08 (stellar)	Clontech	Cat#636766
Biological samples		
Chemicals, peptides, and recombinant proteins		
TbE-Syt-C2B (aa459-594)	This paper	N/A
Critical commercial assays		
Deposited data		
TbE-Syt-C2B structure	This paper	PDB: 7A1R

Experimental models: cell lines		
T. brucei TREU927/4 GUTat10.1	Berriman et al., 2005	https://science.sciencemag.org/content/309/5733/416.long
T. brucei 427 29.13	Wirtz et al., 1999	https://science.sciencemag.org/content/268/5214/1179
Experimental models: organisms/strains		
Oligonucleotides		
Primer: TbE-Syt-C2B Forward: GCAGCTGCATATGAGCACTCGCTCGACGGTGCC	This paper	N/A
Primer: TbE-Syt-C2B Reverse: CGACGGATCCTTAGTGGCGCAGAAGCTTAAG	This paper	N/A
Primer : TbE-Syt-ORF, TbE-Syt-ΔC2B, TbE-Syt-TM Forward : AAAATTCACaagcttATGGAAAAGGCAAATGAACTGATGCA	This Paper	N/A
Primer : TbE-Syt-ORF, TbE-Syt-C2B, TbE-Syt-ΔTM Reverse : CCCGGTACCGGATCCgtggcgcagaagcttaagttcaag	This Paper	N/A
Primer : TbE-Syt-ΔC2B, TbE-Syt-C2A-SMP Reverse : CCCGGTACCggatccgtggttttcaacaccatcatcgttc	This Paper	N/A
Primer : TbE-Syt-C2B Forward : AAAATTCACaagcttatgggggtggaacgcttttcgtc	This Paper	N/A
Primer : TbE-Syt-TM Forward : CCCGGTACCggatccgctggggttgatgagccactc	This Paper	N/A
Primer : TbE-Syt-ΔTM, TbE-Syt-C2A-SMP Forward : AAAATTCACaagcttatggcgaacaatgtccagtggttgaac	This Paper	N/A
Primer : TbE-Syt-mutC2B E492A Forward : ctgaagaacaaagCaactattggggtctc	This Paper	N/A
Primer : TbE-Syt-mutC2B E492A Reverse : GAGACCCCAATAGTTGCTTTGTTCTTCAG	This Paper	N/A
Primer : TbE-Syt-mutC2B D498A Forward : ctattggggtctccgCcccatacgtcaagttac	This Paper	N/A
Primer : TbE-Syt-mutC2B D498A Reverse : GTAACTTGACGTATGGGGCGGAGACCCCAATAG	This Paper	N/A
Primer : TbE-Syt RNAi Stem-loop sense Forward : TGTAAGCTTCAAACTGTTGATGTCCGGTGA	This Paper	N/A
Primer : TbE-Syt RNAi Stem-loop sense Reverse : TGTCTCGAGACTTGACGTATGGGTCGGAGA	This Paper	N/A
Primer : TbE-Syt RNAi Stem-loop antisense and RNAi double promoter Forward : TGTGGATCCCAAACTGTTGATGTCCGGTGA	This Paper	N/A

Recombinant DNA		
Plasmid: pLew100	Wirtz et al., 1999	https://www.sciencedirect.com/science/article/pii/S016668519900002X?via%3Dihub
Plasmid: p2T7TiB-GFP	LaCount et al., 2002	https://www.jbc.org/article/S0021-9258(20)85247-8/fulltext
Plasmid: pET15b	Novagen	Cat. No. 69661-3
Plasmid: MalpET	This paper	N/A
Software and algorithms		
COOT	Emsley, et a., 2004	http://scripts.iucr.org/cgi-bin/paper?S0907444904019158
XDS	Kabsch, 2010	https://onlinelibrary.wiley.com/iucr/doi/10.1107/S0907444909047337
PHENIX AutoSol	Terwilliger, et al., 2009	http://scripts.iucr.org/cgi-bin/paper?S0907444909012098
phenix.refine	Afonine, et al., 2012	http://scripts.iucr.org/cgi-bin/paper?S0907444912001308
ImageJ	Schneider et al., 2012	https://imagej.nih.gov/ij/
JACoP (ImageJ plugin)	Bolte et al., 2006	https://imagej.net/JaCoP
Costes's randomization	Costes et al., 2004	https://www.sciencedirect.com/science/article/pii/S0006349504744392?via%3Dihub
Other		